Schweizerische Eidgenossenschaft
Confédération suisse
Confederazione Svizzera
Confederaziun svizra

Eidgenössisches Departement für
Umwelt, Verkehr, Energie und Kommunikation UVEK

Bundesamt für Energie BFE

Schlussbericht, March 23rd, 2009

Development of Vacuum glazing with advanced thermal properties

Auftraggeber:
Bundesamt für Energie BFE
Forschungsprogramm Energie in Gebäuden
CH-3003 Bern
www.bfe.admin.ch

Auftragnehmer:
Empa, Swiss Federal Laboratories for Materials Testing and Research
Überlandstrasse 129
CH-8600 Dübendorf
www.empa.ch

Autoren:
Matthias Koebel, Empa Dübendorf, Matthias.Koebel@empa.ch
Heinrich Manz, Empa Dübendorf, Heinrich.Manz@empa.ch

BFE-Bereichsleiter: Andreas Eckmanns
BFE-Programmleiter: Charles Filleux
BFE-Vertrags- und Projektnummer: 152950 / 102341

Abstract

Windows constitute a weak link in the building envelope and hence contribute significantly to the total heating energy demand in buildings. By evacuating the glazing cavity a vacuum glazing is created and heat transfer can be significantly reduced. This project was designed to build knowledge and technology necessary to fabricate vacuum glazing with advanced thermal properties. More specifically, various strategies for improvement on conventional technology were investigated. Of central importance was the development of a novel edge sealing approach which can in theory circumvent the main limitation of conventional glass soldering technology. This approach which is rapid, low temperature, low cost and completely vacuum compatible was filed for patenting in 2008. With regards to thermal insulation performance and glazing deflection, numerical studies were performed demonstrating the importance of nonlinear behavior with glazing size and the results published. A detailed service life prediction model was elaborated which defines a set of parameters necessary to keep the expected pressure increase below a threshold value of 0.1Pa after 30 years. The model takes into account four possible sources of pressure increase and a getter material which acts as a sink. For the production of 0.5m by 0.5m glazing assembly prototypes, a high vacuum chamber was constructed and a first sealing prototype realized therein. The manufacture of improved prototypes and optimization of the anodic bonding edge sealing technology with emphasis on process relevant aspects is the goal of a follow-up project supported by the EKZ innovation fund which is currently on its way. This work was funded by the Swiss Federal Office of Energy (BFE).

Zusammenfassung

Fenster stellen eine Schwachstelle in der Hülle eines Gebäudes dar und machen daher den Grossteil der Wärmeverluste darin aus. Wird der innenliegende Zwischenraunm in einem Fenster evakuiert, entsteht ein Vakuumglas und der Wärmeverlust verringert sich deutlich. Das Ziel dieses Projekts war es, Wissen und Technologien zum Bau bzw. zur Realisierung von Vakuumglas mit verbesserten thermischen Eigenschaften zu fördern. Genauer gesagt wurden diverse Strategien zur Verbesserung konventioneller Technologien untersucht. Dabei steht an erster Stelle die Entwicklung eines neuartigen Randverbundssystems bzw. Fügeverfahrens welches theoretisch die Grenzen des heute üblichen Glaslotverfahrens zu durchbrechen vermag. Das von uns entwickelte Verfahren ist rasch und preisgünstig, arbeitet bei deutlich niedereren Temperaturen und ist komplett vakuumtauglich. Die Methode wurde 2008 zum Patent angemeldet. Bezüglich thermischer Isolationsleistung und thermomechanischen Eigenschaften des Vakuumverbundglases wurden rechnerische Studien durchgeführt und die Resultate publiziert. Diese zeigen auf, dass sowohl Gesamtwärmeduchgang als auch mechanisches Durchbiegen des Glases unter thermischer Beanspruchung stark nichtlineares Verhalten aufweisen. Zudem wurde ein Lebensdauermodell aufgestellt, welches eine Auswahl von Parametern definiert, welche über Erreichbarkeit einer Lebensdauer von 30 Jahren Lebensdauer bei einem Druckanstieg unter 0.1 Pa bestimmt. Das Modell berücksichtigt vier mögliche Ursachen des Druckanstiegs sowie das Gettermaterial welches als Senke wirkt. Zur Herstellung von 0.5m mal 0.5m grossen Verbundprototypen wurde eigens eine Hochvakuumanlage geplant und aufgebaut sowie ein erstes Muster darin hergestellt. Die Herstellung von verbesserten Prototypen mit besonderem Schwerpunkt auf prozessrelevanten Faktoren ist das Ziel eines durch den EKZ Innovationsfonds geförderten Nachfolgeprojekts, welches bereits begonnen hat. Diese Arbeit wurde durch das Schweizerische Bundesamt für Energie (BFE) unterstützt.

History and motivation

In Switzerland more than 40% of all energy is consumed in buildings[1], mainly for heating purposes. Windows constitute weak links in the building envelope that exercise a major impact on heating energy demand[2]. The heat transfer mechanisms in gas-filled glazing cavities include radiative exchange between the glass sheet surfaces, convection and gaseous conduction.

The application of two low-emissivity coatings ($\varepsilon = 0.04$) lowers the thermal conductance due to radiation between the glass pane surfaces to roughly 0.1 $W \cdot m^{-2} \cdot K^{-1}$. Even when fill gases such as argon, krypton and xenon are used, thermal conductance due to convection and conduction cannot be reduced significantly below 1 $W \cdot m^{-2} \cdot K^{-1}$. However, if the cavity is evacuated to approximately 10^{-2} Pa or 10^{-4} mbar, heat transfer by convection and gaseous conduction becomes negligible[3,4]. In an evacuated glazing assembly, the total heat transfer rate is determined by radiation and, even more importantly, conduction through support pillars required to bear the atmospheric load on the external glass sheet surfaces. By evacuating the cavity, centre-of-glazing heat transfer rates are achievable that are two to five times lower than those of gas-filled cavities. This translates into energy savings of similar magnitude of installed vacuum glazing compared to state-of the art double glazing for large glazing surfaces.

Modern window technology has made significant improvement since the historic period of singly glazed windows. Double glazing which became standard in the 1970ies cut heat losses in half with typical values of air filled double glazed panes on the order of 3 $W \cdot m^{-2} \cdot K^{-1}$. With the advancement of “heat protection glazing”, the use of low emissivity coatings (low-ε) substantially reduced radiative losses so that air filled double glazing products with U-values below 2 $W \cdot m^{-2} \cdot K^{-1}$ were available on the market in the early 1990ies. Additional improvement of low-ε coating technology and the use of low-thermal conductivity gases (Ar, Kr, Xe) further reduced thermal losses so that current state-of-the-art double glazing slightly below 1 and triple glazing with U-values as low as 0.5 $W \cdot m^{-2} \cdot K^{-1}$ can be obtained. From an economic point of view, triple glazing is disadvantageous because it is too heavy and too expensive for mainstream applications. In addition, the low abundance and related imminent shortage of thermally superior Kr and Xe noble gases on global markets raises questions of affordability for world-wide adaptation and implementation. Vacuum glazing seems the reasonable answer to society’s ever increasing energy consumption and CO_2 output reduction efforts. Depending on the materials used it could in principle be manufactured at a cost similar to that of a conventional double glazing but without the use of rare noble gases and with the added benefit of superior insulation performance.

The potential of the evacuated glazing cavity was realized early on. A number of patents were written on this topic even before 1970 [5,6,7,8]. The great interest in the topic of evacuated glazing cannot be measured only by the increasing number of scientific publications published, but also by tremendous number of new patents published every year which deal with technical solutions and implementations. What in theory seems like a simple endeavor, proved quite complicated to realize over the years: World-wide a great number of technical solutions had been proposed and tested [9,10,11], however even today there is no single double glazed evacuated glazing commercially available which can reach a U-Value of 0.5 $W \cdot m^{-2} \cdot K^{-1}$ or better. Our motivation is to aid in the development of promising new technologies which can further the advancement of a commercial realization of vacuum glazing with advanced thermal properties and life time. This entails simultaneous activities in a number of fields with a clear emphasis on the edge sealing method development.

Project Goals and Milestones:

The goal of this project was to develop the technology required for fabricating high-performance vacuum glazing which is superior to already existing concepts with a predicted service life of > 20 years and by means of processes that are scalable to industrial dimensions and that can be realized cost-effectively. En route to realizing this goal, the following milestones have to be achieved and were defined as the project goals:

- development and demonstration of a technique for fabricating an edge seal with sufficient hermeticity and mechanical integrity
- numerical analysis of heat transfer over the entire glazing assembly
- numerical analysis of the mechanical behaviour of the glazing assembly
- service life analysis based on leakage measurements of prototype assemblies and simulations
- fabrication of a roughly 0.5m x 0.5m prototype glazing assembly including support pillars and getter

Final goal and brief summary: The successful completion of the proposed program should have resulted in the demonstration of a new technology superior to existing concepts. The envisioned glazing will possess a center-of-glazing thermal transmittance of 0.5 $W \cdot m^2 \cdot K^{-1}$ or less, a value which is significantly lower than currently available evacuated glazings. The prototype should demonstrate the ability to maintain that reduced thermal transmittance over extended periods of time. All goals were met within the project timeline with exception of the last milestone which was only partially completed due to unexpected problems with the solder dispensing. This aspect is now the main focus of research in a follow-up project funded by EKZ, the canton of Zürich's electrical grid company.

Development and demonstration of a technique for fabricating an edge seal with sufficient hermeticity and mechanical integrity

The ideal sealing approach

By far the most important technological challenge related to vacuum glazing manufacture is the development of a proper edge sealing technology. For this reason, most of the project resources and time were spent on the advancing this aspect. Despite the fact that there are many research groups worldwide working on one and the same task, the edge seal is still the main obstacle for a practical realization of vacuum glazing. Probably the most widely used approach nowadays is sealing of two glass panes with a glass solder. There are many disadvantages associated with this concept which we want to improve on with a new and more innovative sealing method. Glass solder sealing requires high temperatures (450˚C - 500˚C) applied over periods of several hours[12] including heating and cooling down to ambient temperature. Such high temperatures are also not compatible with low-ε coatings and tempered glass, which from the start disqualifies such a window from ever reaching U-values below 1 $W \cdot m^{-2} \cdot K^{-1}$ because radiative heat transfer is limiting the overall performance. In addition it is a non-vacuum compatible technology which means that the seal is made first under atmospheric conditions and the glazing is evacuated later through a pumpout tube. This does not only add an extra step in the production process but it is impractical for large glazings due to a rapid loss of pumping speed at reduced pressures with increasing distance from such a tube. In addition, this technology renders surface cleaning virtually impossible which raises serious doubts regarding the resulting service life limitations.

Significant improvement over current technology can be achieved, if the following criteria are met. In other words, an ideal sealing approach must have the following process features:

- low process temperature[13] to prevent damage to low-ε coatings and to prevent loss of tempering. An ideal sealing temperature would be between 250°C and 350°C because outgassing of the glass panes *in vacuo* requires elevated temperatures.
- sealing *in vacuo*: A “seal and forget” process eliminates evacuation through pumpout tube and the related problems.
- surface cleaning (UV/ozone or sputtering) and baking of individual glass panes in a vacuum environment separated by a minimum distance of 10cm eliminates performance limitations due to photofragmentation reactions and long-term outgassing respectively.
- a fast process is essential for economical large-scale production.

Only an integral approach which combines all of those features can guarantee “advanced thermal properties” of the manufactured product as claimed in the title of this work. To the best knowledge of the authors, there is currently only one parallel approach being developed in Germany as part of the Pro-VIG project network which satisfies all of the requirements of an ideal sealing approach stated above.

Anodic bonding

Anodic bonding can produce mechanically strong connections between an insulator and a metal without the need for sample pretreatment or activation. The anodic bonding of various conductive materials to glass has been described for the first time in 1969 by Wallis and Pomerantz[14]. They demonstrated the formation of an irreversible bond between different metals or semiconductors and an ion-containing glass by applying a potential between the two materials and heating them at to relatively low temperature (250℃ – 400℃).

The idea of using a metallic seal and the possibility of "low-temperature" (< 350℃) and simultaneous hermetic bonding to two glass panes motivated us to test this technique as a sealing method for vacuum glazing. An initial study was designed as a proof of principle experiment earmarked by simplicity and rapid setup time.

First experiments

All experiments were carried out under standard atmospheric pressure without inert gas protection. The effect of the bonding parameters, such as bonding time and applied voltage was crudely monitored. This initial series of experiments was a feasibility test of anodic bonding and was carried out in an ambient air environment:

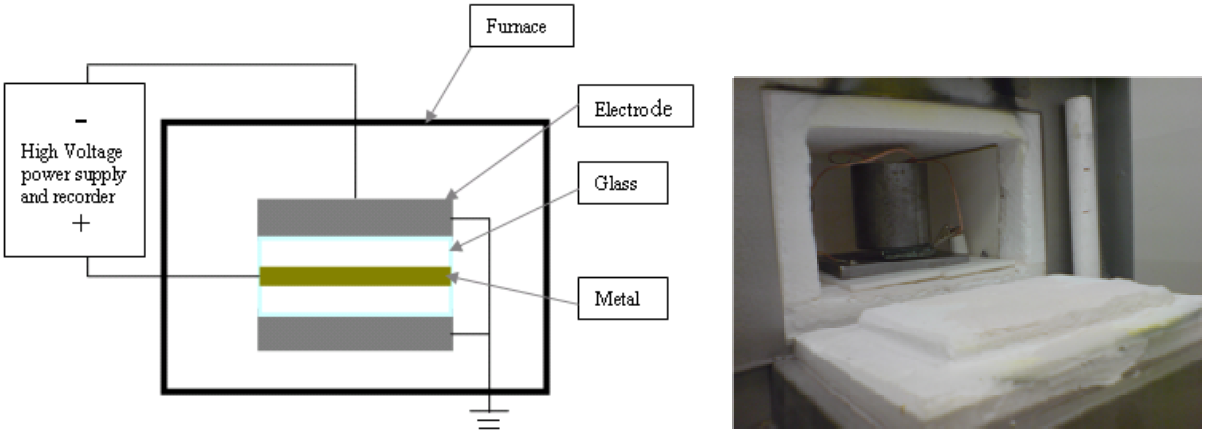

a) b)

Fig. 1 a) Schematic diagram of experimental setup for anodic bonding experiments in air. b) Furnace used for anodic bonding experiments in air.

It is known from various reports that Aluminum forms a tough bond with soda-lime glass when bonded anodically[15,16]. Contrary to a conventional single-interface anodic bonding experimental setup, the approach used here was that of a double sandwich anodic bonding i.e. two glass-metal interfaces were bonded simultaneously. A schematic of the double-field assisted bonding setup is given above in Figure 1 a): A metal foil is sandwiched in between two pieces of glass which were cut to approximately 3cm · 3cm dimension. The foil was connected to the positive lead of a HPx 10158 high voltage power supply (ET power system Ltd), which can deliver voltages from 0 - 1000V and output currents 0 - 1500mA. The glass/metal/glass assembly was again sandwiched in between two copper electrodes which were held at ground potential. Typically +800 volts were applied to the metal creating a strong electric field between glass and metal which is necessary for the bonding to take place. During the bonding process, both voltage and current were controlled and monitored

by means of a computerized data interface. The entire setup was placed inside a ceramic furnace (see Figure 1 b)) which could be heated up to 600°C.

Prior to the experiment, glass and metal were washed with acetone and ethanol to remove surface contaminants. Once prepared, the sample was placed inside the furnace and the electrical leads were connected. The system was then heated to temperature (typically between 250-350°C) and the positive voltage was applied to the metal with the glass being held at ground potential. The high voltage was turned off after the current had dropped to zero. A schematic of such temporal temperature and corresponding I/V profiles is given in Figure 2. After the system was cooled to room temperature, the bonded specimen was removed from the furnace.

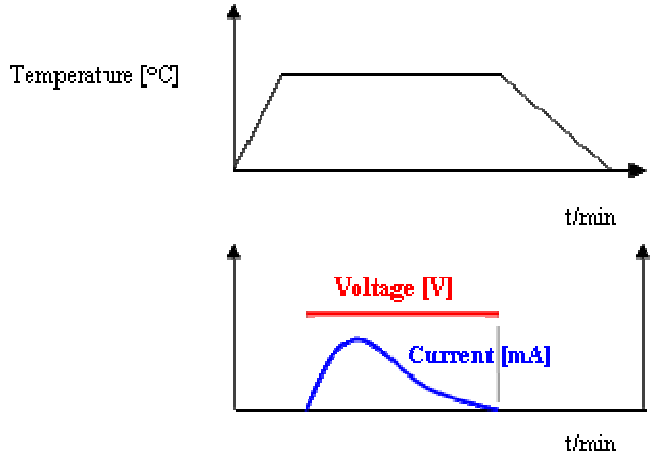

Fig. 2 Typical current / voltage / temperature profiles: Following heating to temperature, the voltage is applied. The current first rises sharply and then decays exponentially. Once it reaches zero, the sample is cooled to room temperature.

In order for the anodic bonding process to occur, a closed circuit between anode and cathode is required for a chemical reaction to take place. Hence, charge equilibration of redox species involved in the electrochemical half-cell reactions at the electrode interfaces is essential. That means that there needs to be a net transport of charge through the glass substrates. This charge equilibration is affected through transport of ions under action of the applied electric field. From a kinetics point of view, charge equilibration by ionic transport is rate-limiting for the overall anodic bonding reaction. Hence, the glass needs to be a good ionic conductor at the sealing temperature for maximum bonding performance. This is why glasses with high network modifier contents (Na^+, K^+, Ca^{+2}, Mg^{+2}) such as float glass are ideal for anodic bonding to metals. Table 1 shows the typical chemical composition of standard float glass which is virtually identical in composition with soda-lime glass:

Component:	SiO_2	B_2O_3	Al_2O_3	CaO	MgO	Na_2O	K_2O	Softening point
% composition	73.0	0.0	1.0	8.5	3.5	13.5	0.5	~ 570°C

Table 1 Typical chemical composition of float glass (mass percentages)

Note that standard window float glass typically contains no borate or phosphate network formers. For our first set of experiments, 30µm thin aluminum foils were bonded to 3cm by 3cm, float glass squares of 4mm strength at 300°C. After a few initial tests the formation of a strong bond between the glass sheets and the Al foil was confirmed. In a second experiment,

a 5mm hole was drilled into one of the to glass squares prior to assembly and an Al frame was cut out from 30μm foil and placed in between. The first test specimen fabricated in this way shown in Figure 3 a) and b) was leak tight with a leak rate smaller than the sensitivity limit ($2 \cdot 10^{-10}$ mbar $\cdot$ $l^{-1} \cdot s^{-1}$) of our He leak testing device. Leak testing and ultrasonic interface analysis are the primary characterization tools which were used to test for seal hermeticity and integrity.

A Helium leak testing device detects leaks by measuring the He gas penetrating into or emerging from a test object. Helium gas flowing through a leak due to a pressure difference between the inner and the outer space of the test object is then detected by a mass spectrometer. This type of leak testing is the most sensitive method of detection commonly used in vacuum technology[17]. Ultrasonic inspection[18] avails itself of high frequency ultrasonic (acoustic) pulses. Sound waves generated by a transducer are coupled to the inspection piece and propagate through the material. If there is a discontinuity (such as a crack or delaminated interface) in the wave path, part of the acoustic wave will be reflected back from the flaw surface. Reflected wave components arrive back at the transducer/receiver unit at a time which uniquely defines the position of the discontinuity. In our case, two dimensional scanning allows imaging of the bonding interface integrity. In the ultrasonic image, the false-color coding from blue to red represents integral bonding with the two surfaces in intimate contact (blue, no reflection of ultrasound waves at the bonding interface) to complete disbonding (red, reflection due to an interfaces discontinuity. This sample shows some defects which could be due to air inclusions; however no end-to-end leakage channel or discontinuity is apparent in the ultrasonic image.

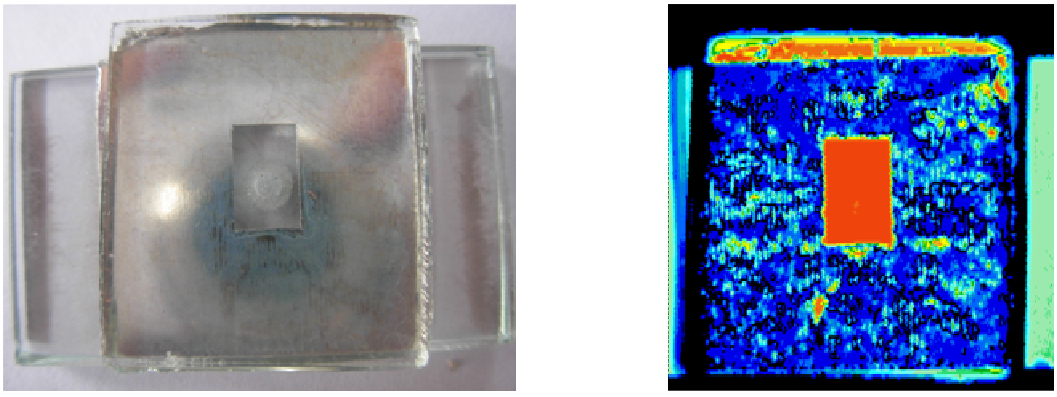

a) b)

Fig. 3 a) photographic (left) and corresponding b) ultrasonic (right) image of a sealing specimen fabricated by the simultaneous anodic bonding of 30μm Al foil frame to two pieces of glass.

Edge sealing *in vacuo*

Initial results from experiments conducted in air were quite promising. As an alternative to aluminum, tin-based solders are potential candidates to be investigated further. In air, liquid tin-based alloys are prone to rapid surface oxidation. There is a good possibility that the oxidation problem is reduced significantly if experiments are conducted in a vacuum atmosphere i.e. if oxygen were to be excluded from the bonding process. Also, the importance of the glazing assembly *in vacuo* was pointed out earlier. For those reasons we opted to build a high vacuum (HV) test chamber for the fabrication of small sealing specimens to gain experience with sealing under high vacuum conditions and to test the feasibility of the method and the materials used. All sealing experiments described from here on have been carried out under HV conditions ($p < 8 \cdot 10^{-4}$ mbar).

Setup and procedure

An improved vacuum anodic bonding test setup was designed and constructed. Figure 4 a) shows its main components (vacuum chamber and turbomolecular pump, temperature controller, high-voltage power supply and computer for controls). The central components in Figure 4 c) are again electrodes and the glass/metal/glass assembly which make up the dual "sandwich" anodic bonding experiment. The difference to the previous setup is first the fact that everything is placed inside a small vacuum chamber (see Figure 4b)) and second that the two copper electrodes are heated resistively and temperature controlled by two type K thermocouples. The metal seal is connected to the positive lead of a HPx 20157 high voltage power supply (ET power systems Ltd.), which delivers up to 150mA of current at a maximum voltage of 2000V. The chamber can be pumped down to a base pressure of approximately $5 \cdot 10^{-4}$ mbar by means of a Pfeiffer / Balzers turbo pump stand within less than 5 minutes. The temperature controlled heaters provide sufficient heating energy (2 x 100W) to heat the sandwiched setup to a maximum temperature of 400°C within less than 10 minutes. The high voltage power supply is controlled via PC interface which allows the user to define and run voltage profiles and record I/V data simultaneously.

a)

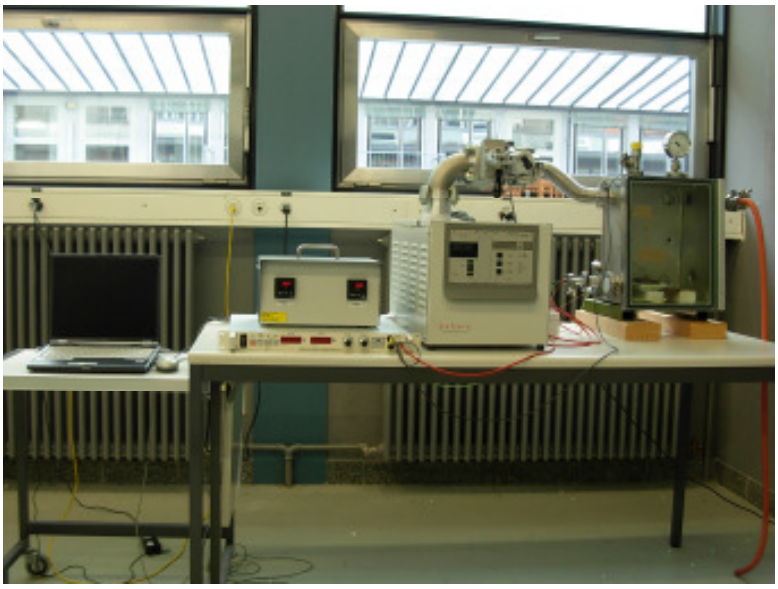

b)

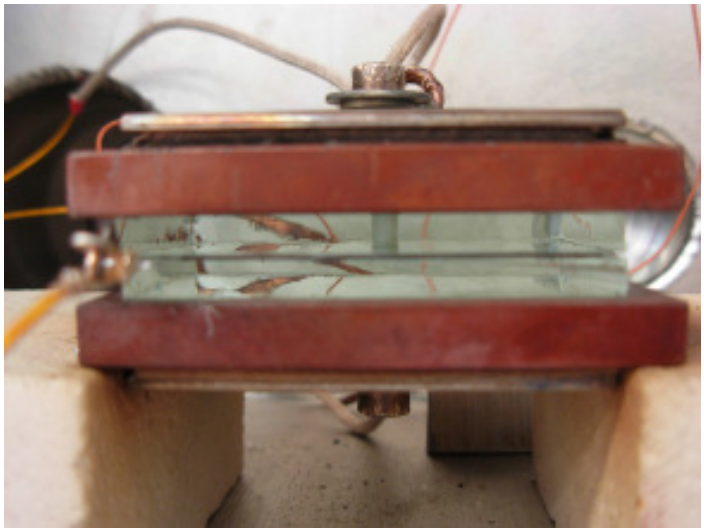

c)

Fig. 4 Photographs showing a) the complete bonding test setup, b) the vacuum chamber and c) a close-up view of the bonding specimen featuring metal seal, glass slides and heated electrodes.

Classical anodic bonding: aluminum and float glass

A number of experiments were conducted on the Al / float glass system. A central question to be answered in the first instance was whether the anodic bonding method is vacuum compatible and if additional complications occur in a vacuum environment. Voltage control was greatly facilitated because of a newly developed I/V profile recording program which enabled us to record temporal current/voltage (I/V) profiles. From the integrated I (t) curve, the total amount of transported charge could be extracted. The total amount of charge transported is one key parameter when discussing bond strength and performing bonding parameter optimization studies. Analogous to the samples fabricated in air, ~1cm wide Al-frames (250µm sheet and 30µm foil) especially designed for the fabrication of prototype seal specimens (see Figure 5 a) and b)) were cut out and anodically bonded to two matching 5cm by 5cm float glass pieces. Again one glass featured a 3mm-diameter hole for leak testing of the assembly.

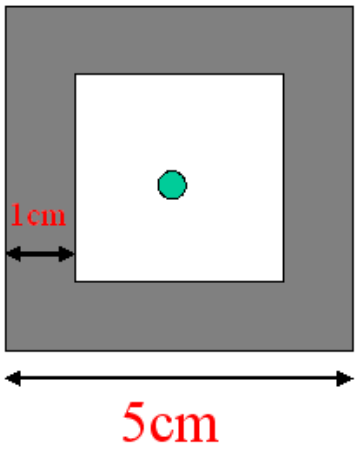

Fig. 5 a) Schematic illustration of Al-frame

Fig. 5 b) 250µm Al-sheet specimen

In preparation of the anodic bonding experiment, two 250µm thick sheet aluminum frames were polished with 1µm grain size diamond polishing suspension and pressed under 600KN force. This procedure was used to ensure flatness of the Al surface which facilitates the contact of glass and metal surfaces during bonding. All components were rinsed with acetone/ethanol prior to assembly to remove surface contaminants. Following the pretreatments, the assembly was heated and anodically bonded in a high vacuum environment of ~$5 \cdot 10^{-4}$ mbar for 15 minutes after the set temperature had been reached.

In analogy with experiments conducted in air, Al was found to bond strongly to float glass with the majority of samples showing extreme integrity when bonded at 800V for 10 minutes at a temperature of 250°C - 350°C. Mechanical loading of strongly bonded samples resulted in fracture in the glass rather than along the interface indicating satisfactory bond strength for vacuum glazing edge sealing application.

Over a temperature range from 250°C to 350°C, the bonding kinetics varied substantially as evidenced in the shape and peak maximum of the I(t) curves (see Figure 6) of the three samples shown below: Identical 250µm Al sheets gave rise to highest peak values and fastest decay of the measured currents when bonded at 350° (highest T).

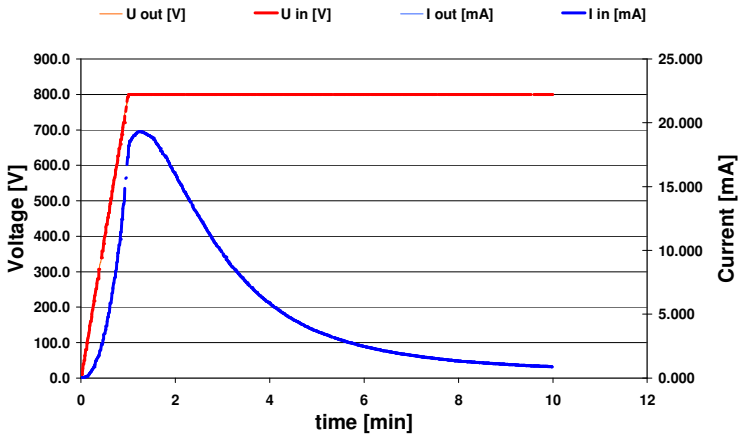

Fig. 6 a) I(t) profile of 250µm-Al specimen bonded at 350°C

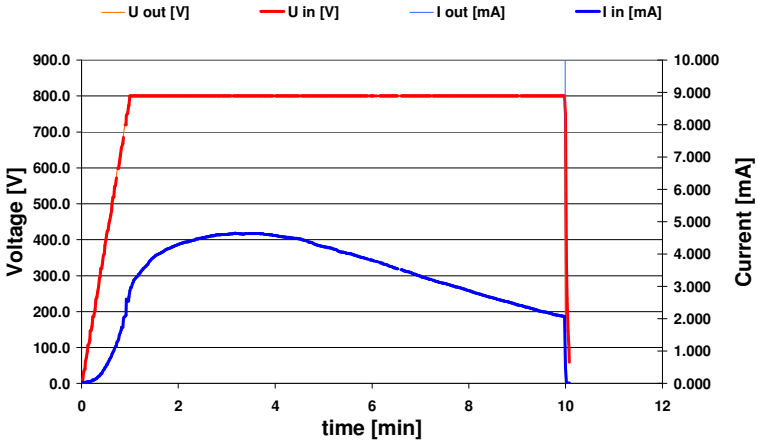

Fig. 6 b) I(t) profile of 250µm-Al specimen bonded at 300°C

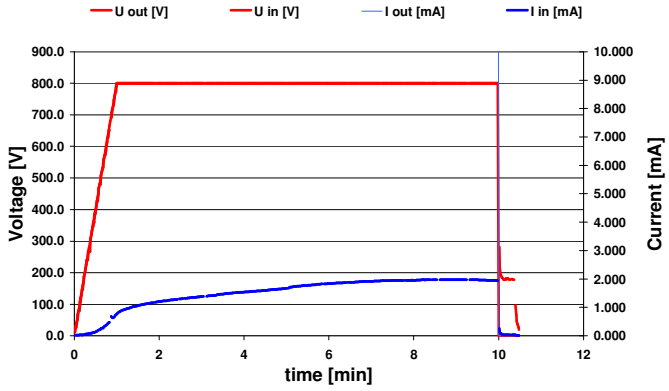

Fig. 6 c) I(t) profile of 250µm-Al specimen bonded at 250°C

Bonding at 250°C on the other hand, was associated with a roughly 10 times smaller peak current but much slower rise and decay of the I (t) curve; the 300°C is somewhere in between the two extremes. The peak current I_{max} decreases with temperature and the time to reach I_{max} termed t_{max} increases with decreasing temperature. We are convinced that this effect is due to a kinetic limitation of the transport of ions by electromigration across this interface. In anodic bonding there are two main phenomena controlling the overall bonding process. First, there is anodic oxidation of the metal anode, in this case Al and the corresponding reduction reaction at the cathode. Second, Al^{+3} ions which are formed during

the oxidation step will diffuse to the glass and alkali and earth alkali cations in the glass in close proximity to the cathode will electro-migrate to that electrode under the action of the applied electric field. The extent or rate of this second process is limited by the ionic conductivity of the glass. In other words, charge transport (diffusion) of cations in the glass which is necessary to complete the electrical circuit and equilibrate the total charge is rate-limiting and depends strongly on the glass temperature. This explains the difference in the transient current profiles observed at various temperatures.

Uniform contact issues

Despite substantial efforts made to guarantee uniform surface contact of the aluminum and the glass surfaces, non of the 250µm Al-sheet specimens were leak tight, with typical He-leak rates on the order of $5 \cdot 10^{-6}$ mbar $\cdot l^{-1} \cdot s^{-1}$. The formation of a leak-tight seal which satisfies the stringent conditions for VG application, requires a very flat and smooth metal seal surface in perfect contact with both glass panes. The presence of minute cracks, bends or scratches provides a channel for air to leak through which is detected by both, leak testing and ultrasonic inspection.

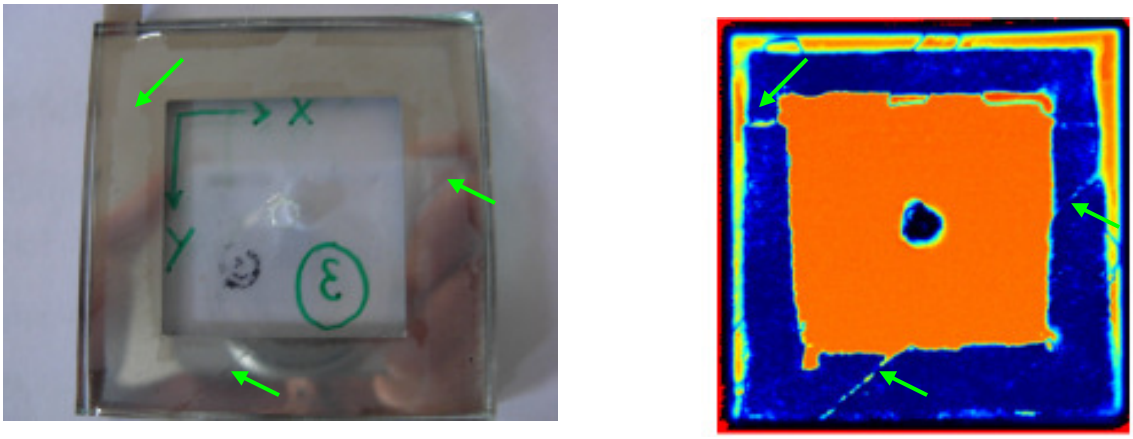

Fig. 7 250µm Al sheet test-frame bonded at 300°C and its corresponding ultrasonic image

Unfortunately, we were not able to produce a leak-tight seal from commercial aluminum sheets which satisfy those requirements with reasonable effort. This is underlined by the fact that all 250µm Al frame specimens manifested cracks (→) in the ultrasonic images (see Figure 7). Table 2 shows a summary of experimental parameters for the three 250µm Al-sheet frame samples. Note that the current transport characteristics I (t) vary significantly with temperature; this is attributed to the increase of the ionic conductivity of glass with temperature as discussed above.

No. of specimen	T [°C]	I_{max} [mA]	ρ_{max} [mA·cm^{-2}]	t_{max} [min]	He leak-rate [mbar · l^{-1} · s^{-1}]
S1	350	19.30	0.60	1.27	$8 \cdot 10^{-6}$
S2	300	4.64	0.15	3.78	$5 \cdot 10^{-6}$
S3	250	1.92	0.06	9.35	$3 \cdot 10^{-6}$

Table 2 Characterizations of 250µm Al sheet specimens S1, S2 and S3 which were anodically bonded at different temperatures with 800V applied for 10 minutes. The maximum current density is termed $\rho_{max} = I_{max} / (2 \cdot S)$ where in this case S ~ 16 cm^2 is the seal frame bonding area.

In order to inspect the interface of the joint, scanning electron microscopy (SEM) was used. Figure 8 shows a selection of secondary electron (SE) images recorded at 20keV beam energy. For electron microscopy analysis, square pieces of approximately 1cm by 1cm dimension were cut out from the original samples using a Struers sectioning saw (cutting speed = 10mm/minute) and a Si-C blade. Cross-sectional samples were then embedded into epoxy glue, ground to a 600-grit finish and polished with 3µm and finally 1µm diamond polishing suspension. Prior to SEM analysis, polished cross-sectional samples were coated with a carbon layer to minimize charging effects.

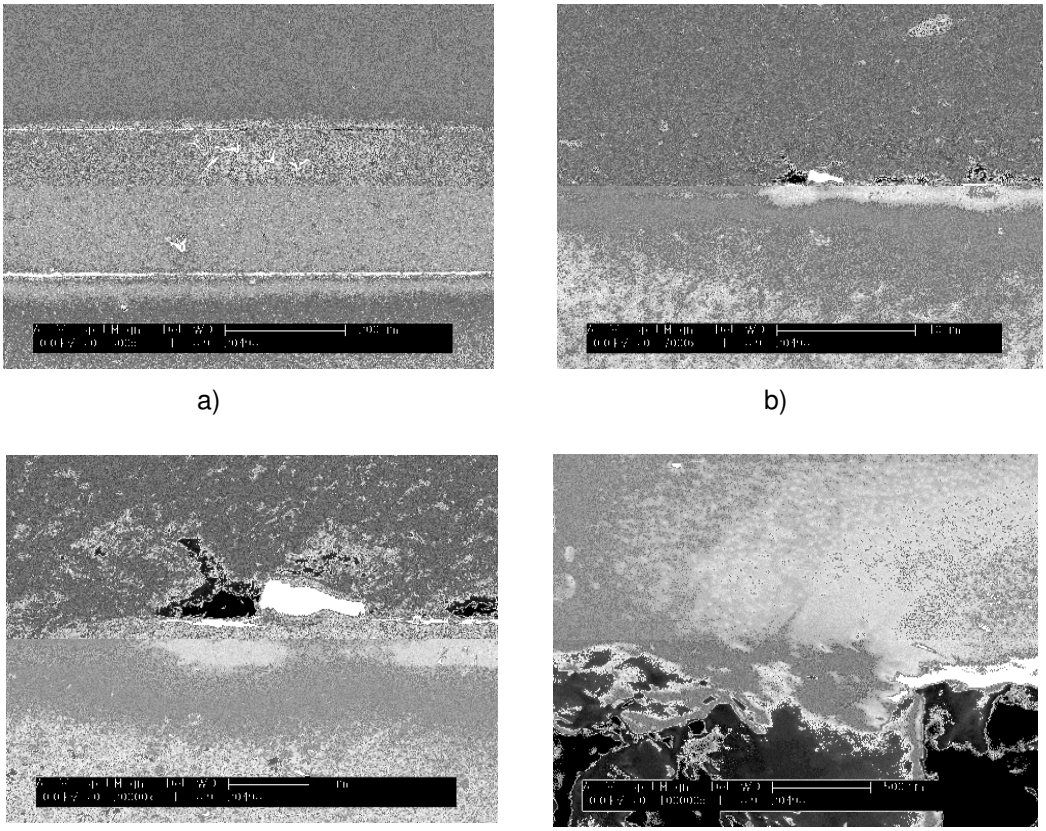

a) b)

c) d)

Fig. 8 a) through d) SEM images of glass/Al interface made from sample S1 made from using a 250µm sheet bonded at 350°C: a) overview, b) bonded interface with defect, c) same interface defect zone with larger magnification, d) high resolution image of defect interface

In Figure 8 a) one can see an overview of the entire interface: The aluminum sheet is double-sandwich bonded inbetween two pieces of glass. Because glass is harder and more abrasion-resistant than aluminum, more defects on the aluminum metal surface from polishing are apparent. In Figures 8 b) and c), a magnified section of the glass/Al interface is shown with the Al metal on top. Along the interface, some holes are observed. The presence of holes alone does not exclude the sample from being leak tight because there needs to be a continuous leakage path from outside to inside i.e. over several millimeters. Nevertheless, the presence of too many interface defects is undesirable and can weaken the bond which makes it more susceptible for failure. At the interface on the glass side, approximately 0.6µm away from the interface, we observe an approximately 0.6µm-wide strip which appears brighter in the SE image. Figure 8 d) shows a bonding defect or hole in the Al-layer of the interface in more detail at 100'000 X magnification.

Alternative to the 250µm sheet, a frame cut out from 30µm Al foil was used to manufacture analogous sealing specimens. Bonding was carried out under identical conditions i.e. *in vacuo* at 350°C and with a voltage of 800V applied. I_{max} reached 19.90 mA after t_{max} of approximately 4 minutes. Interestingly enough the current peaked twice as shown in Figure 9, perhaps due to improved surface contact of a previously noncontacting larger area after ~3.5 minutes.

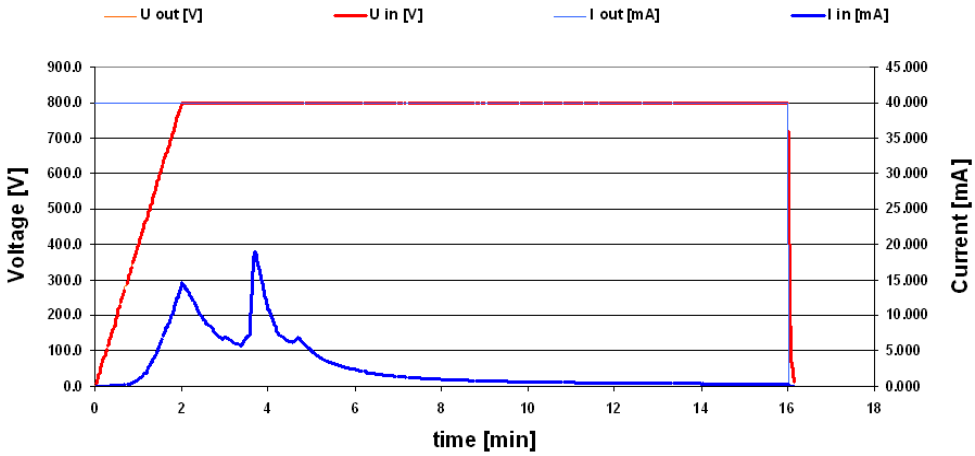

Fig. 9 I(t) profile of a 30µm-Al foil specimen bonded at 350°C

A photographic and the corresponding ultrasonic image of the 30µm foil sample are shown in Figure 10. This specimen was leak tight with a leak rate below the sensitivity limit ($2 \cdot 10^{-10}$ mbar $\cdot$ $l^{-1} \cdot s^{-1}$) of our leak testing device and this despite a significant number of bonding defects. The clear difference between this sample and the previous 250µm sheets is that the defects were small and randomly distributed. They did not form a continuous path for air to leak through such as the previously mentioned cracks.

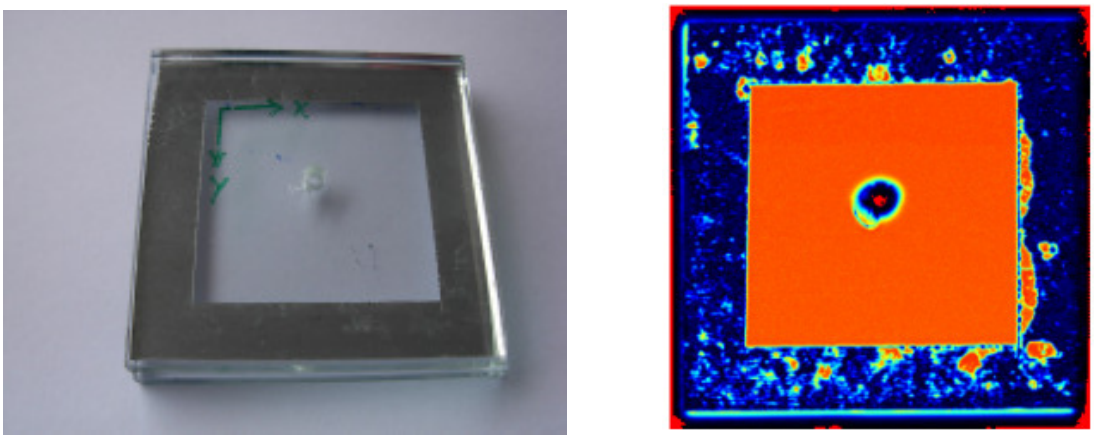

Fig. 10 30µm Al foil test-frame and ultrasonic image

Again, SEM was used to probe the interfaces between the 30µm Al foil and the glass. Two typical images are shown in Figure 11 below.

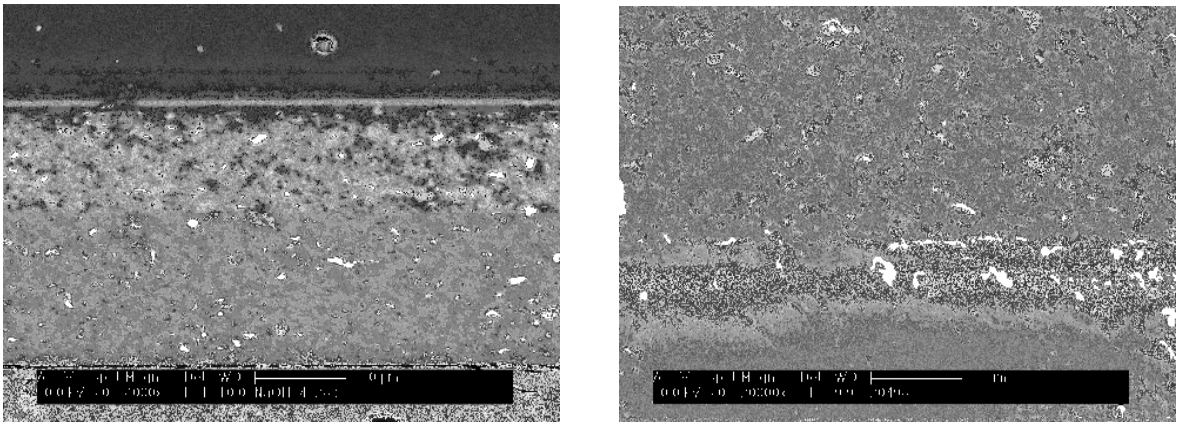

(a) (b)

Fig. 11 SEM pictures of interface of 30µm Al foil/glass joint: a) overview and b) bonded interface area (Al on top)

Figure 11 a) again shows the overview of a double sandwich bonded glass/Al/glass specimen. No obvious interfacial defects along the entire interface length were observed, even upon closer SEM inspection (20'000X magnification, Fig 11 b)). In analogy with the SEM images taken from the 250µm sheet 350°C bonded specimen S1, a brighter strip in the glass interface was observed. EDS mapping confirmed that this strip corresponds to an area of increased earth alkali ion (Ca^{+2}, Mg^{+2}) concentration. Migration of ions in an electric field causes rarefaction and concentration zones similar to separation effects used in chromatography or electrophoresis.

To conclude, we were able to verify that anodic bonding between Al and float glass works quite well in a high vacuum environment and the formation of strong bonds is observed or in other words, that the presence of large amounts of molecular oxygen is not necessary for bond formation. In the case of the 30µm foils, leak-tight samples of 5cm by 5cm dimension with a measured leak rate $< 2 \cdot 10^{-10}$ mbar $\cdot$ $l^{-1} \cdot s^{-1}$ could be manufactured. Analogous glass/Al/glass frame specimens made from 250µm Al sheets showed large area defects in the form of channels and were not leak tight. A possible explanation lies in the mechanical properties of the metal sheet. The bending stiffness for a thin plate depends to the third power on the plate thickness according to the classical plate equation. This means, that the

elimination of kinks or bends from a 250µm Al sheet necessary to guarantee simultaneous intimate contact with both glass surfaces requires roughly $(8.3)^3$ ~ 570 times higher pressure than if a 30µm foil is used. Apparently, even the 600kN pressing was not enough to even out the kinks in this case. This set of experiments confirms that a gap of a quarter millimeter cannot be sealed by an aluminum sheet without leakage, a problem which is amplified even more in the case of glazings of typical window dimensions with significantly larger circumference. This excludes anodic bonding of Al sheet frames as a practical sealing technology for vacuum glazing. In addition, the fabrication of metallic seals of such dimensions and the requirement of a seal to be manufactured from a single workpiece (large Al-sheet) would mean a tremendous amount of waste and render the process useless from an economic point of view.

Liquid tin solder anodic bonding

From previous experience, we have learned that Al can form strong anodic bonds in conjunction with float glass. However, Al-sheets cannot yield leak-tight joints over larger dimensions with reasonable effort. Again, the main reason for this problem is the mechanical stiffness of Al which results in insufficient surface contact, one of the main factors determining quality and hermeticity of anodic bonds. For the sake of finding a candidate metal or alloy which could adapt better to the glass surface during the bonding process, tin based soft solder alloys such as SnAg3.5‰$_m$, SnAg3.5Cu0.5‰$_m$ shall be considered. Given their low melting points between 217°C and 221°C, bonding in the liquid state is going to be attempted. Alternatively, the process temperature can be kept just below melting which means that the solder is still in the solid state but considerably softer than for example the Al foil. The goal of a first study is to demonstrate the anodic bonding of Sn-based solders in the liquid state and find evidence for improved surface contact.

A first set of solder frame specimens from SnAg3.5Cu0.5‰$_m$ with a melting point of 217-220°C were manufactured by bending and overlapping a solder wire to produce a square frame (see Figure 12) and pressing it with a hydraulic press (F = 600kN) analogous to the preparation procedure used for the Al sheets in the previous section. The sample was placed inside the high vacuum chamber and the system evacuated to a base pressure of $5 \cdot 10^{-4}$ mbar and heated to a temperature of 260°C. Much to our surprise no current was observed *in vacuo* when 800V volts were applied, even after 10 minutes time. After waiting for one additional hour, current began to flow and peaked at about 0.5 mA. The minimal bonding current clearly came as a surprise. When looking through the transparent glass chamber door, it was difficult to tell whether the solder had melted or not, even though the electrode temperatures were significantly above the melting temperature of the solder. We then suspected that slow melting was due to thermal equilibration processes in vacuum being much slower than in air. Under HV conditions heat transfer through gaseous conduction is suppressed (the same effect one tries to take advantage of in a vacuum glazing) and both, first the glass and then the solder, are heated indirectly by mostly radiative heat transfer and some bulk conduction at a few points which are in direct mechanical contact. In order to speed things up and to achieve higher bonding currents by raising the ionic conductance of the glass, the process temperature was increased to 300°C. As expected, melting of the solder took significantly less time. Anodic bonding at a voltage of 800V applied after 20 minutes at this temperature led to peak currents of approximately 1.2mA within 10 minutes.

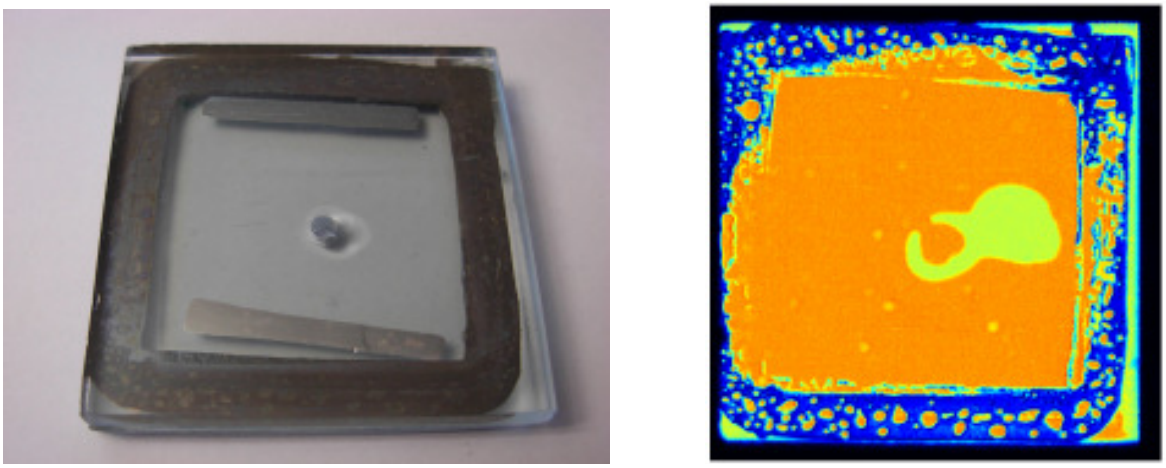

Fig. 12 SnAg3.0Cu0.5 m% frame specimen *in vacuo* and its corresponding ultrasonic image

All specimens produced in this manner did not exhibit satisfactory bond strength. This was evidenced by the fact that they were easy to crack open by hand, some of them even fell apart by themselves. Breakage always occurred directly at the interface indicating that this was the weakest point. Not surprisingly, not a single leak-tight specimen could be fabricated in this manner. Typical measured He-leak rates were ~ 10^{-6} mbar · l^{-1} · s^{-1} for 5cm by 5cm square samples. A great number of holes in the bulk of the solder are visible in both the photographic and more clearly the ultrasonic image. This phenomenon can be attributed to poor wetting of the glass surface by the solder, air trapped in the solder which evolves upon melting of the solder under high vacuum conditions or the chemical evolution of gases during bonding.

Another soft solder material SnAg3.5%$_m$ which is commonly used as a lead-free solder and commercially available, was tested for anodic bonding *in vacuo*. This alloy was received in the form of 150µm thick sheets which we attempted to bond both as a frame and also as a 5cm by 5cm square. Specimens were assembled as usual and heated to 300°C *in vacuo*. After waiting for ~20 minutes, a minute amount of current (~ 0.1 mA) was observed with 800V applied. At that time, the anodic bonding process was started and the voltage kept at said value for 10 minutes. The current rose slowly to reach a peak current density $\rho_{max} < 0.03$ mA · cm^{-2} and then decayed exponentially. A typical “whole area” and a frame specimen are shown in Figures 13 and 14 respectively. Again, many bubbles in the bulk solder were visible indicating poor solder homogeneity and perhaps outgassing.

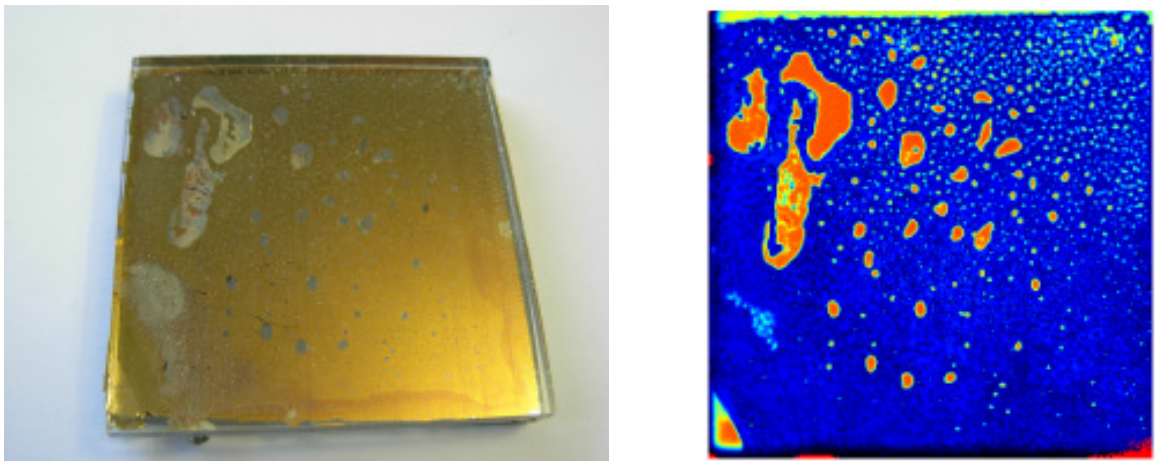

Fig. 13 Whole area SnAg3.5%$_m$ solder specimen and corresponding ultrasonic image

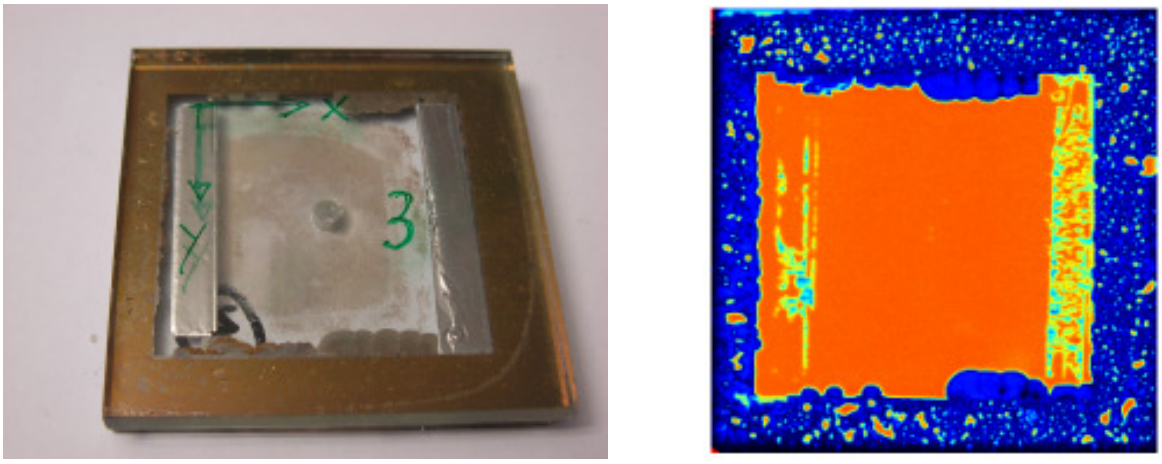

Fig. 14 SnAg3.5‰$_m$ solder frame specimen and corresponding ultrasonic image

SnAg3.5‰$_m$ specimens disbonded along the interface as well when exposed to small mechanical loads or by themselves. Measured He leak rates were on the order of 10^{-6} mbar $\cdot$ l^{-1} $\cdot$ s^{-1}. The frame specimen in Figure 14 shows small silver-gray areas on the top and bottom inner edges of the frame where liquid solder was squeezed out and had adapted to the glass surface uniformly without bubbles. This is a somewhat encouraging result because it suggests that (degassed) solder could be injected from the side and produce a continuous frame without holes or bubbles.

To conclude, we were able to demonstrate that SnAg3.5‰$_m$ and SnAg3.0Cu0.5‰$_m$ soft solder can be anodically bonded to glass, however producing mechanically weak seals. Because of that weak bond strength, we infer that $SnAg_{3.5}$ and $SnAg_{3.0}Cu_{0.5}$ solders are ill-suited for VG hermetic sealing. The main advantage of the tested sheets and frames made from tin-based solder alloys is a clearly improved surface contact in the areas where solder is still present which can be seen in the corresponding ultrasonic images. However, many bubbles are observed introducing huge amounts of defects into the bonded interface and producing leaky seals. The squeezed-out solder adapted to the glass even more uniformly and more importantly in a “bubble-free” manner. A promising next step is to find a suitable low-melting solder candidate which fulfills not only the criterion of adaptation to the glass surface in the liquid state but also forms a mechanically strong bond with glass.

Activated tin solder

SnAg and SnAgCu solders were disqualified because of the mechanically week joint formed with glass. Three main reasons for the unsatisfactory mechanical strength can be the formation of a significantly thick passivating oxide layer during melting and prior to the anodic bonding step, poor wetting of the glass surface and the formation of a mechanically weak mixed oxide with the glass (SnO_2 – SiO_2) at the bonding interface. Another suitable alloy which could bring improvement over the previously tested solders on the two latter counts is quasi eutectic SnMg2‰$_m$ (2 mass percent Mg) with a melting temperature T_m of ~212°C. Figure 15 below shows the binary phase diagram of Sn and Mg.

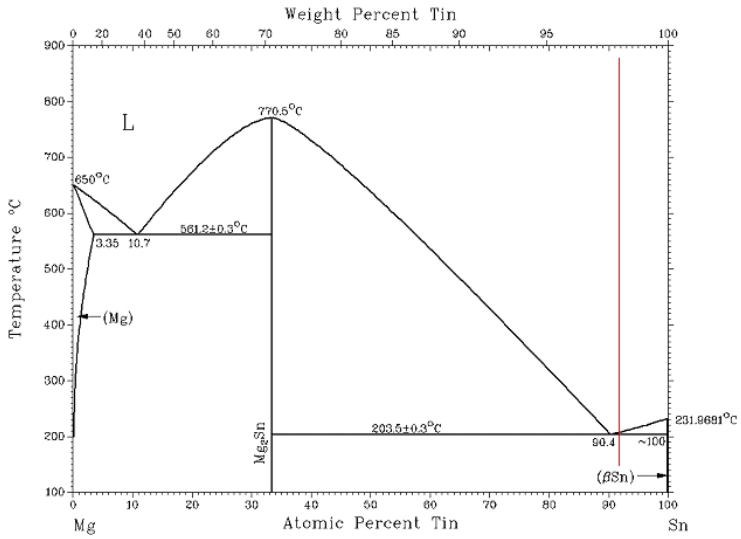

Fig. 15 Phase diagram of the Tin-Magnesium bimetallic system

In a preliminary test study, a square piece of SnMg2%$_m$ alloy was pressed to ~5cm^2 square flat pieces under 600KN force. Following a crude surface cleaning pretreatment with acetone/ ethanol of the alloy and glass surfaces, the glass/alloy/glass sandwich assembly was anodically bonded *in vacuo* (p = 5·10^{-4} mbar) with 1000 volts applied. During our initial trials, specimens were bonded at 300°C. In two out of two cases, arcing was observed leaving behind a burnt spot in the glass and causing the current to spike quickly to its maximum value set by the current limiting hardware after around 4 min (see Figure 16 a) and b)). Generally the arcing problem is reduced, when the bonding is carried out at a lower temperature or voltage. A specimen bonded at 250°C / 1000V produced a 0.12 mA·cm^{-2} current density at a peak current I_{max} of 1.1mA but did not arc.

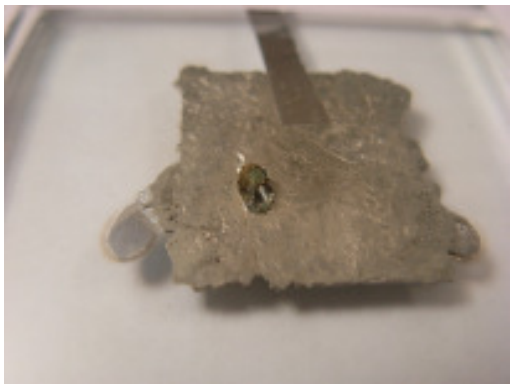

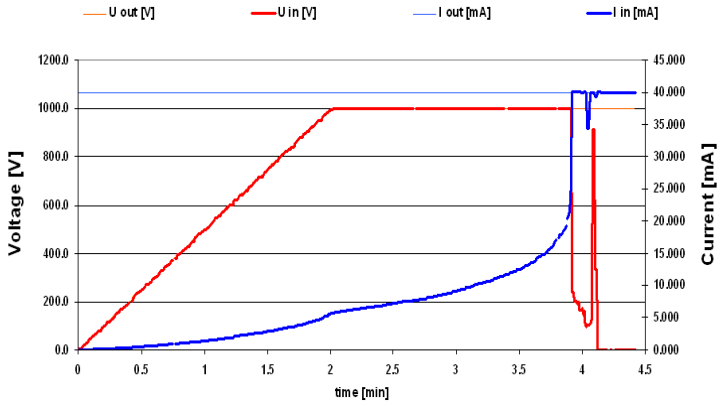

a) b)

Fig. 16 SnMg2%$_m$ specimen: a) evidence of arcing and b) corresponding I(t) profile showing the arcing event

Through optimization we evaluated the ideal arcing-free bonding conditions for this system as 280°C / 1000V and observed 4.0 mA of peak current which translates into an average current density of approximately 0.25 mA·cm^{-2}. A picture of this specimen and the corresponding ultrasonic image is shown on the next page in Figure 17. Even though the recorded temperature is ~70°C higher than T_m, the SnMg2%$_m$ alloy melts only partially and slowly. Just like in the previous tin solder experiments, part of the liquid alloy was squeezed out to form a fresh and metallic looking area, which again shows little defects in the

ultrasonic image compared to the original coin-shaped piece. Again, we attribute the discrepancy between the recorded temperature (representative of the Cu-electrode temperature) and T_m and the slow melting of the alloy to poor heat transport in vacuum between the Cu-electrode and the glass surface and finally the solder alloy coin. The bonded alloy adapted reasonably well to the glass surface with a clear contrast in the ultrasonic image to the background.

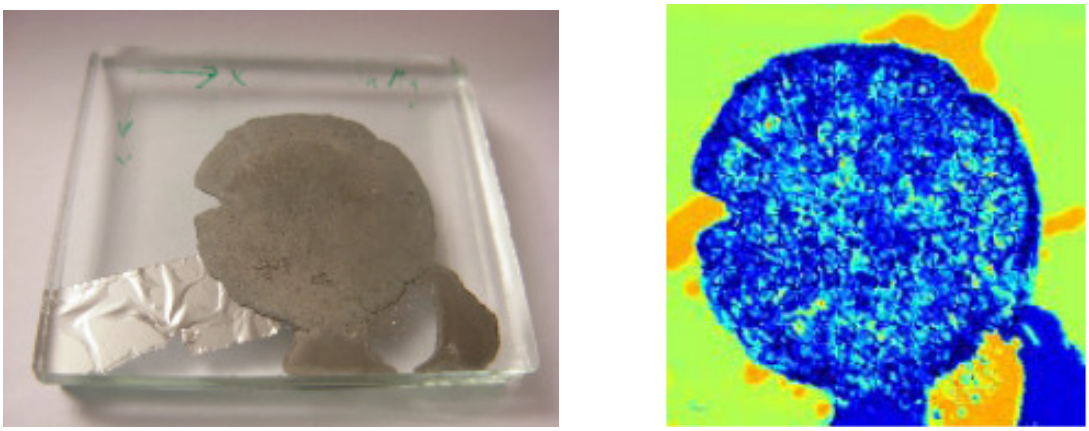

Fig. 17 SnMg2%$_m$ specimen bonded at 280°C: Photograph and corresponding ultrasonic image

Some frame specimens were also made from pressed SnMg2%$_m$ wire and tested using the same optimized conditions. Unfortunately, no leak tight specimens could be obtained in this way. One of the main reasons is probably the fact that a large part of the solid alloy did not adapt to the glass surface perfectly, most probably because of the formation of an oxide/layer which appears grayish dark on the original solder workpiece after the reaction. In addition, this area displays many holes and defects in the solder bulk, leaving passage ways for air to leak through.

As far as the mechanical toughness of the joints is concerned, loading tests were made on some randomly selected specimens. All SnMg2%$_m$ samples broke relatively easily and still along the interface, however the interfacial strength was significantly improved compared to the previously tested SnAg3.5%$_m$ and SnAg3.0Cu0.5%$_m$ specimens. We believe that the presence of a relatively thick oxide layer limits prevents the formation of a decent anodic bond in this case and that areas which are bonded with freshly squeezed out liquid alloy material are predestined to performing much better.

The element distribution at the bonding interface was again investigated by SEM/EDS. A secondary electron (SE) image and EDS maps of the elements Mg, Si and Sn are shown in Figure 18. The SnMg2%$_m$ alloy is shown on top and the glass below. This coincides with the respective Sn and Si element maps in Figure 18 c) and d). Analogous to the Al samples (see for example Figure 8 b) and c) or Figure 11 b)), a bright, ~0.8µm wide strip at the glass-solder interface was observed on the glass-side in the SE image Figure 18a). More importantly, significant enrichment of Mg at the bonding interface (on the glass side) is evident in the Mg element map b) in the form of a strip of similar width as the one seen in the SE image. This is attributed to anodic oxidation of Mg and diffusion of Mg^{+2} cations into the glass. The fact that Mg^{+2} is migrating across the interface and into the glass, suggests, that Mg is playing an active role in the bond formation as an activating component. It proves that Mg is surface active and gets oxidized (electrochemically) to form Mg^{+2}. The detailed mechanism of the bond formation is still poorly understood and will be the focus of future studies.

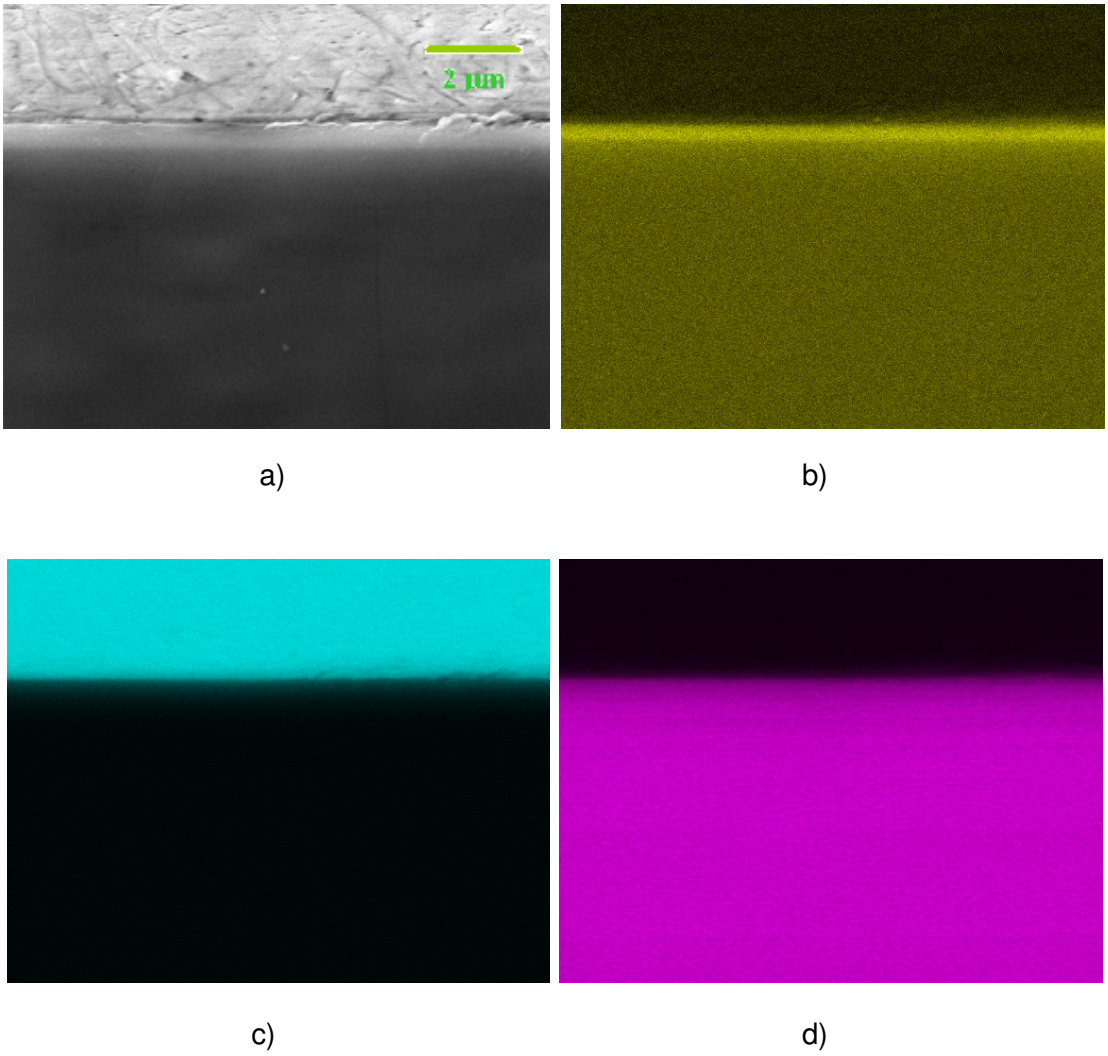

Fig. 18 SEM image and EDS maps of interfacial area of SnMg2%$_m$ specimen: a) secondary electron (SE) image, b) Mg, c) Sn and d) Si EDS element distribution maps

Unfortunately, all sealing material candidates which had been tested this far were not ideal for VG sealing: the aluminum sheet bonds to glass strongly but not in a leak-tight fashion. SnAg3.5%$_m$, SnAg3.0Cu0.5%$_m$ and SnMg2%$_m$ soft alloys bond to glass but exhibited insufficient bond strength and did not produce hermetic seals. As an alternative to Mg, which was the most promising material tested so far, Al could be a suitable candidate as an activating component. The problematic of rapid oxidation as it was observed in the case of Mg could be reduced because Al forms, at least in its pure metallic state, a thin film of a protective oxide layer only a few nanometers thick which halts further oxidation of the bulk metal. Second it is well known that Al forms extremely strong anodic bonds with glass and we demonstrated that the activating component Mg exhibited high surface activity. If the same is to be true for Al, the SnAl system could indeed be a promising solder material for anodic bonding to glass.

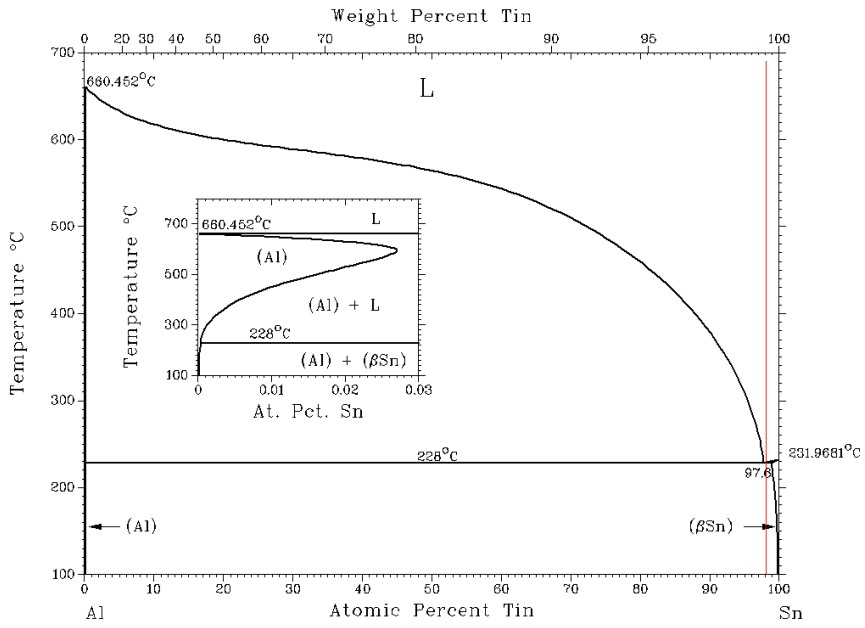

Fig. 19 Phase diagram of the Tin-Aluminum bimetallic system

The binary phase diagram in Figure 19 reveals a small eutectic gap at approximately 0.6%$_m$ Al in Sn. The melting temperature of this alloy (232°C) is still low enough to be useful for our intended anodic bonding approach. An initial set of experiments involved a few ~5cm^2 coin-shaped SnAl0.5%$_m$ alloy pieces pressed to ~250µm thickness which were bonded to two 5cm by 5cm standard float glass squares. We again determined a set of optimized bonding parameters for this system: At least a 10 minute waiting period was necessary to observe melting after the electrode temperature of 300°C had been reached. Then, a voltage of 800V was applied for 16 minutes and the sample allowed to cool to room temperature. Most of the specimens fabricated in this way showed extremely tough bonds: large loading forces were required to break the samples and rupture occurred partially along the glass and partially inside the glass with small glass shards sticking to the solder alloy metallic gasket. This indicated that the fracture energy required to break the glass is of similar magnitude than the toughness of the glass itself. A photographic image of a typical sample is shown in Figure 20.

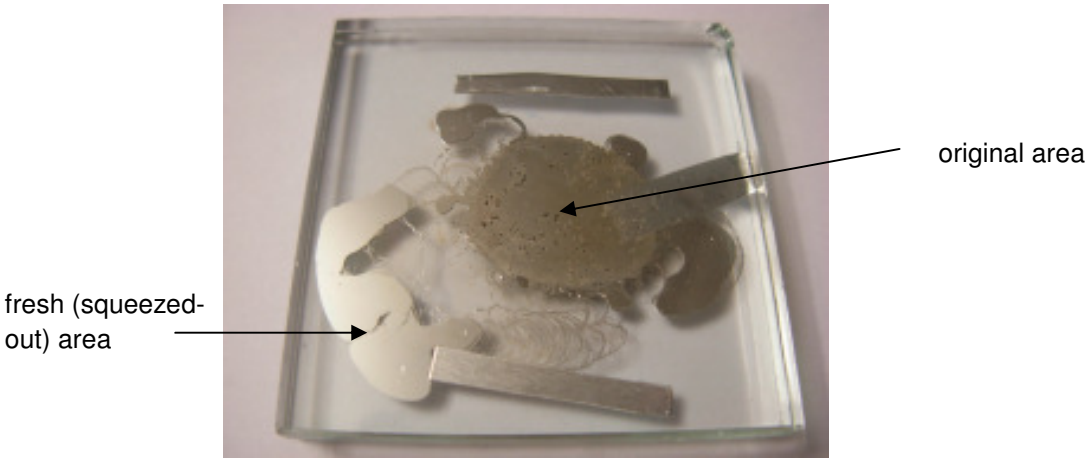

Fig. 20 Photographic image of a specimen made from a coin-shaped SnAl0.5%$_m$ solder alloy

Peak bonding currents I_{max} of about 12 mA (!!) were reached for a total active area of 20cm^2. This value of I_{max} translates into a peak current density of approximately 0.6mA·cm^{-2}, more than twice the value observed in the case of SnMg alloys. This difference we attribute to improved activity of the Al metal over Mg and the presence of a thicker oxide layer in the latter case which impairs the bonding reaction. The SnAl bonded sample shows two distinctly different parts as well: a greyish "original" area with bubbles at the interface and a shiny fresh area composed of "squeezed out" solder material. A closer inspection of loading ruptured interfaces showed that the original was disbonded exclusively along the interface and within the solder itself, most likely because of reduced mechanical integrity in the bulk material because of holes and because of the presence of surface contamination (oxides, carbonaceous materials) which weakened the interfacial bond. The "squeezed out" fresh area alloy was malleable and tough after melting and solidification and rupture occurred quite often within the glass indicating strong bonding with few defects. In addition, this area showed a perfect metallic and mirror-like surface.

After the initial coin-shaped $SnAl_{0.5}$ m% specimens, some frame samples were fabricated as well. First, four 4cm-long wires were pressed under 600kN force to make a frame (~250µm thick). Following assembly of the glass/solder frame/glass (one glass with a 3 mm hole for leak testing) had been assembled, the specimen was anodically bonded at 300°C / 800V and $5 \cdot 10^{-4}$ mbar. The specimen photo and corresponding ultrasonic image are shown in Figure 21 below. Many bubbles are observed in the original frame area, but the shiny "squeezed out" fresh area again shows virtually no bulk defects. The SnAl solder seemed to adapt to the glass well and bond uniformly. It did not come as a surprise, that none of these frame specimens, fabricated in the same way as the specimen shown in Figure 21, proved to be leak tight with typical He leak rates on the order of 10^{-6} mbar $\cdot$ l^{-1} $\cdot$ s^{-1} given the large volume fraction of holes observed in the majority of the bulk solder.

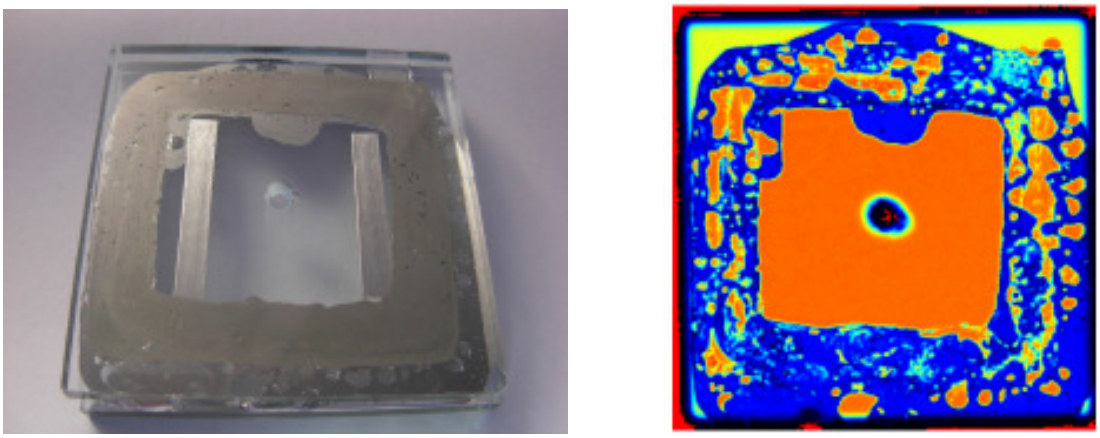

Fig. 21 Photographic image of a specimen made from a coin-shaped SnAl0.5 m% solder alloy

For closer inspection of the glass/ $SnAl0.5\%_m$ alloy joint interface SEM/EDS electron microscopy was conducted on an "original" and a "fresh" region cross section cut obtained from a coin-shaped SnAl bonded specimen (300°C / 800V). The images are shown in Figure 22 (SEM) and Figure 23 (EDS).

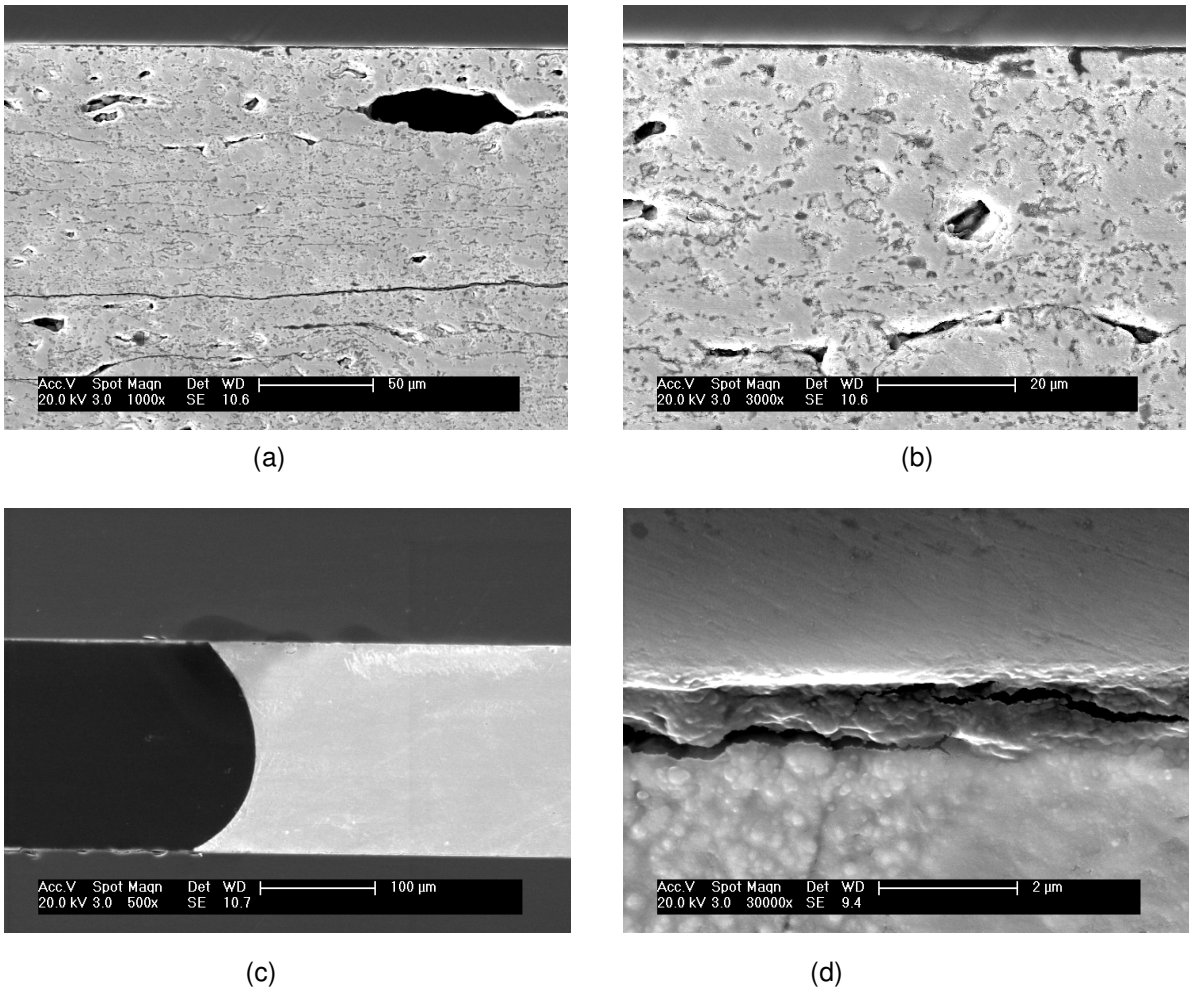

Fig. 22 SEM images of a typical SnAl0.5‰$_m$ anodically bonded sample: Original area [top, a) bulk metal microstructure, b) bonding interface] and freshly squeezed out solder area [bottom, c) contact angle and overview, d) bonding interface]

Figure 22 a) and b) both display the “original” solder area. The glass side appears on the top and the SnAl0.5‰$_m$ alloy on the bottom. The microstructure contains many defects (holes, cracks) in the bulk and a long discontinuity along the glass/metal interface as seen in the magnified image in b). Image 22 c) show a wetting contact angle between “fresh” SnAl0.5‰$_m$ and the two glass sheets of ~30°. This indicates good adaptation of the SnAl0.5‰$_m$ alloy to the glass surface under action of the electrostatic force; this contact angle must not be interpreted as a wetting condition in the traditional sense because wetting only occurs upon application of the electric potential and there are electrostatic forces at play. Compared to the original area, much fewer defects in the “fresh” solder bulk are observed which is commensurate with our ultrasonic inspection results. A high resolution image of the “fresh solder” area shows good interfacial contact and the possibility of cracks, perhaps due to thermal stresses and/or effects during sample preparation (cutting, embedding, grinding and polishing).

The element distribution at the bonding interface was again recorded by EDS. In Figure 23, a SE image and EDS maps of the elements Al, Sn and Si are shown with the SnAl0.5‰$_m$ alloy on the top and the glass at the bottom of the image / maps. This matches again the distribution of Sn and Si elements shown in c) and d) expected for metal and glass. Analogous to previous experiments involving Al-metal sheets and foils as well as SnMg2‰$_m$ solder, a brighter strip is observed in the glass at the interface in Figure 23 a), but this time of

smaller width (~0.25µm). This is primarily the result of the diffusion and enrichment of the active component Al which is seen in the EDS map in Figure 23 b). The Al concentration at the interface must be significantly larger than that of Ca or Mg since the width of the bright strip seen in the SE image represents mostly the Al enrichment zone. From these results we conclude, that significant amounts of Al^{+3} ions formed by anodic oxidation (evidenced by the large bonding current) migrate into the glass under the action of the electric field during the anodic bonding process. This observation counts as strong evidence for the activating role of Al in the bonding process. The narrower width of the enrichment strip is most likely due to a reduced mobility of the Al^{+3} cation compared with Ca^{+2} or Mg^{+2}.

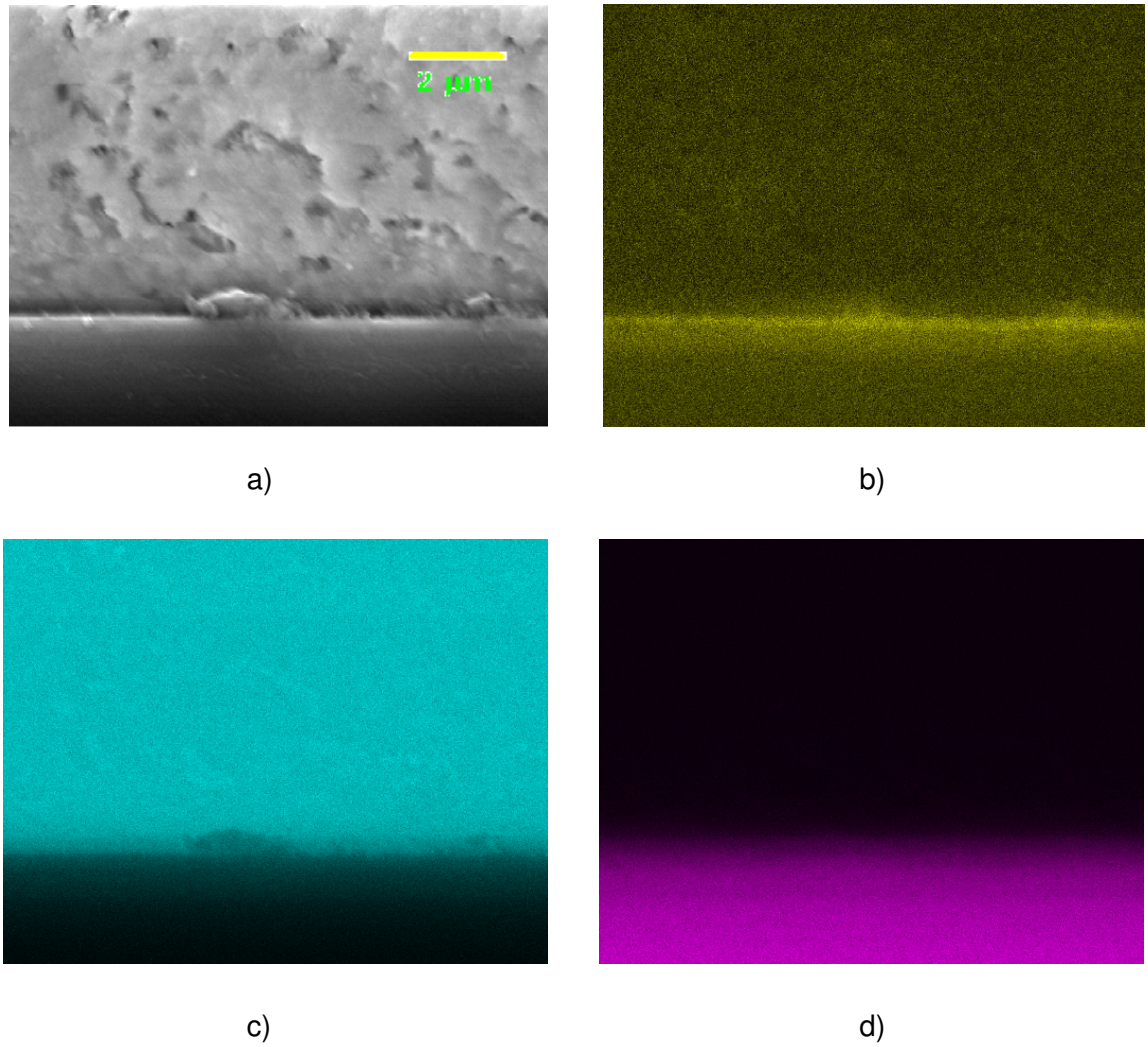

Fig. 23 EDS maps of "fresh" interfacial area of SnAl0.5%$_m$ specimen after anodic bonding: a) SE image, b) Al, c) Sn and d) Si EDS element distribution maps

For comparison, a SnAl0.5%$_m$ "non-anodically bonded" reference sample was fabricated as well. This specimen had undergone identical treatments as the anodically bonded counterpart discussed above, with the only difference that no voltage was applied. Figures 24 and 25 show selected SEM images and an Al EDS map. Many defects are observed in the original bulk microstructure in Figure 24 a) and a large crack along the interface is evident in the magnified region b). It seemed that glass and alloy did not bond together along the most part of the interface. Just like in the anodically bonded case discussed above, the "fresh" area displays much fewer defects than the "original" area. A wetting angle of approximately 120° between alloy and glass is seen in Figure 24 c), which in this case means that the liquid SnAl0.5%$_m$ alloy did not wet the glass significantly. Because wetting

and spreading of molten solder on the glass surface is a prerequisite of effective joint formation between the two materials, the interface between alloy and glass in this case is expected to be weak. This was confirmed by rupture along the interface of the reference sample upon application of small mechanical loads comparable to ones required to break anodically bonded non-activated tin solder alloy samples. Nevertheless, there is some residual bonding of the pure SnAl alloy in the absence of an applied field which is worth mentionning. A patent by the Nippon sheet glass company[19] describes the soldering without prior metallization on float glass with Al, Si or Ti activated Sn/Zn alloys and without voltage (no anodic bonding). However we believe that the mechanical strength of joints produced in this way is not enough to withstand stresses and cyclic loading conditions as they are present in vacuum glazing assemblies subjected to real-life conditions. The fact that no commercial products using this technology have appeared on the market thus far (patent filed march of 2000) suggests that our assumption is correct.

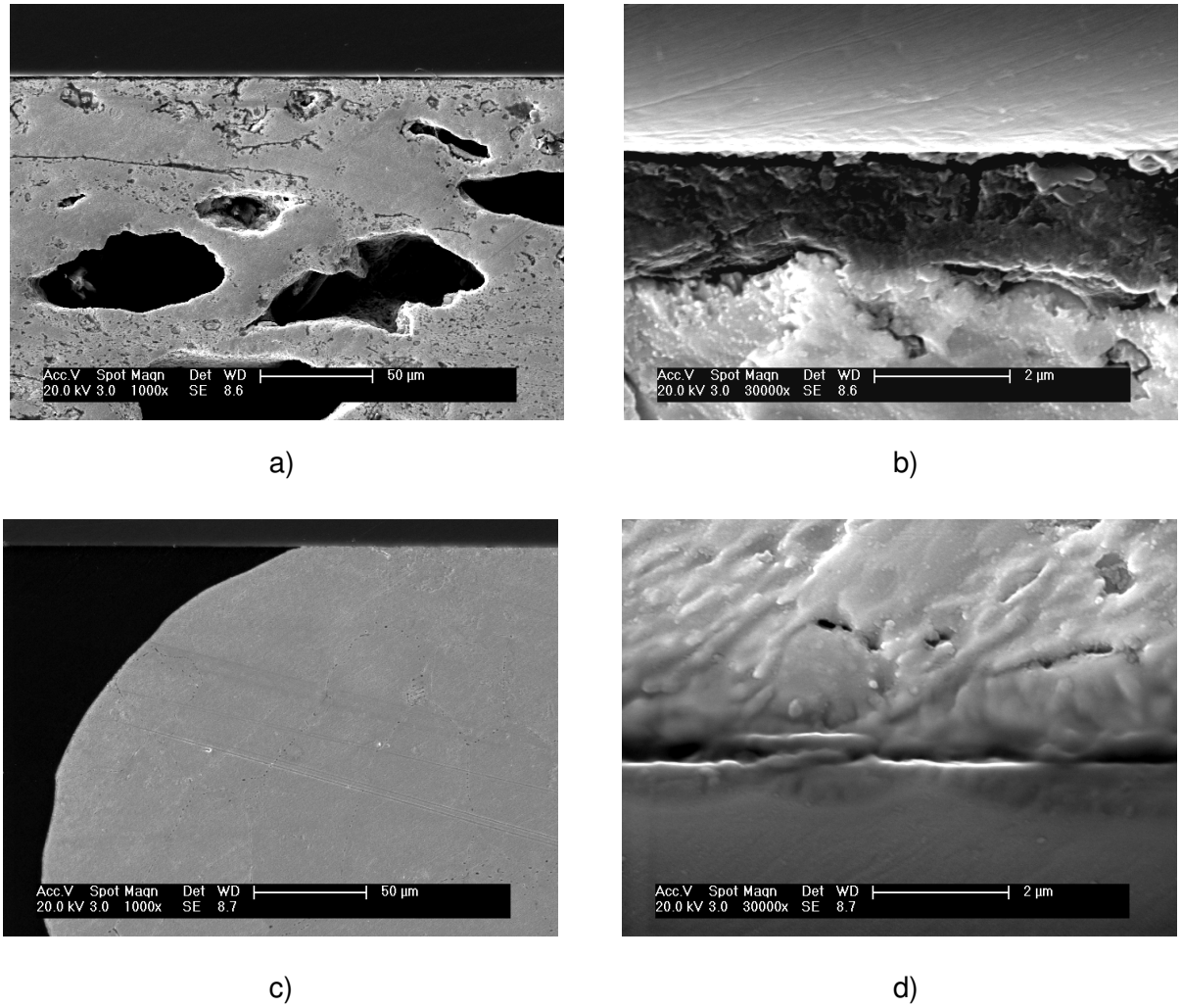

Fig. 24 SEM images of a SnAl0.5‰$_m$ reference sample without any voltage applied: Original area [top, a) bulk metal microstructure and interface, b) enlarged interfacial area] and freshly squeezed out solder area [bottom, c) contact angle and overview, d) solder/glass interface]

Not surprisingly, without the electrostatic force supplied by application of an external electrical potential, no electrooxidation, diffusion and enrichment of the element Al can be observed in the glass adjacent to the SnAl alloy (see Figure 25). Two bright blobs are seen in the solder phase at the interface in the Al-EDS map. We believe that these are islands made from pure Al which precipitates out at this interface during the solidification of the alloy, because Al is insoluble in Sn and does not form stable intermetallic compounds. These Al

islands may be the reason for the residual bonding which is observed without the electric field: Al can form a mixed oxide with the glass in the presence of small amount of oxygen or oxides. These Al-metal islands can then adhere to the glass with relatively decent bonding strength and act as “anchoring” points for the solder. Consequently, it seems feasible that the direct bonding with activated tin-solders to glass in absence of an applied electrical potential is promoted by a multitude of small activator metal islands. However this mechanical connection relies entirely on a small fraction of the total area which is effectively bonded. In other words, there is only a small fraction of the total area, which is actively joined to the glass and which contributes to the total bond strength making this a weakly bonded system. Additional investigations are necessary to verify this theory for the SnAl system.

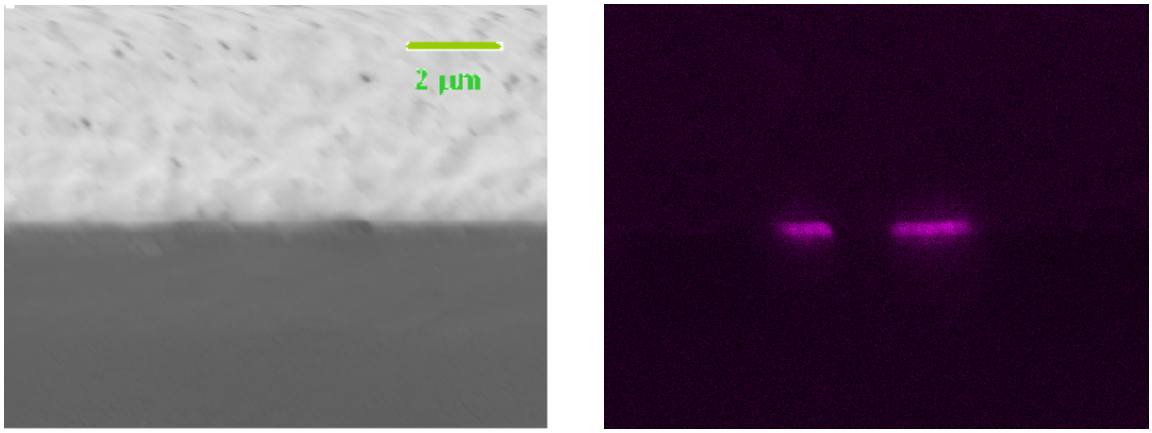

Fig. 25 SEM image (left) and EDS map (right) of “fresh” interfacial area of a SnAl0.5‰$_m$ reference sample with no voltage applied

Our combined results suggest that the anodic bonding process is necessary to supply a mechanically strong bond which is coined over the entire contact area. Conventional activated SnAl “soldering” to glass shows bond strengths which are most probably insufficient for VG applications. At the same time, a new key question arises, namely how to selectively fabricate a seal which consists only of “freshly squeezed-out” blank solder. It is this fresh area which adapts to the glass surface most uniformly and at the same time provides maximum bonding strength.

Solder dispensing pretrials

An initial study with the goal to fabricate oxide-free “fresh” areas of solder entailed the design and construction of a liquid solder dispenser which was based on a commercial ERSA 350W large solder iron. Basically, a cartridge was custom-built to fit into the resistive heater element of said iron. This cartridge was then fitted with an Ar-purge tube and filled with chunks of SnAl0.5‰$_m$ solder. Following a purge cycle with Argon gas, the solder was heated in an inert gas atmosphere (to prevent oxidation) and dispensed through an interchangeable nozzle. The following procedure was elaborated to produce solder frames: previous to the experiment, small pieces of SnAl0.5 m% solder were cleaned with Acetone/Ethanol to remove contamination and used to load the heated cartridge. The iron was then plugged in and the solder was heated until melting occurred. Then, the flow of liquid solder was controlled by regulating the Ar-gas flow / overpressure. Finally, a frame was made by moving the bottom glass (see Figure 26) and extruding a line of solder onto the glass workpiece. After many trials, more or less uniform frames, composed of any desired tin-based solder material, could be obtained.

Fig. 26 Photographic image of the liquid solder dispenser operating in air

Next, two spacers were placed onto the bottom glass and a second glass slide of identical dimensions featuring a 3mm hole was placed on top of the freshly fabricated solder frame. This assembly was then placed into the vacuum chamber and prepared to be anodically bonded in much the same way as done previously. Following evacuation to $5 \cdot 10^{-4}$ mbar, the sandwiched specimen was heated to 300°C. 18minutes after the set temperature was reached, 1500 volts were applied for only 90 seconds; a peak current of 8.25mA was obtained for ~ 14 cm2 bonding area (corresponding to a current density of ~ 0.6mA·cm^{-2}). A photograph of the sample and its corresponding ultrasonic image is shown in Figure 27 below. It seems the solder adapts glass surface well, however there is still some grayish discoloration in the area of the original wire positions and there is a “squeezed-out” fresh area as well.

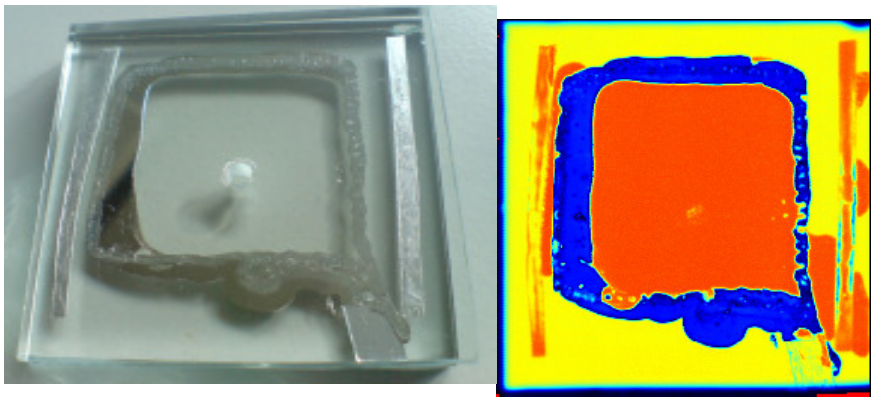

Fig. 27 Photographic (left) and corresponding ultrasonic image (right) of a leaktight specimen made from a SnAl0.5‰ alloy frame extruded by means of the liquid solder dispenser

Leak testing showed a tight seal with a leak rate of $2 \cdot 10^{-10}$ mbar $\cdot$ l^{-1} $\cdot$ s^{-1}. There are again some bubble-like defects which are clearly seen in the ultrasonic image on the right hand side solder-line. The solid solder connection in this area is extremely thin in some places (<100µm) so that it is indeed very encouraging to see the samples hermeticity confirmed in this case. These results indicate on one hand, that a wire containing minimal amounts of surface oxide could work as an edge seal, however it also raises the question of holes and defects: For a larger sealing perimeter, the probability for a critical defect increases if the original solder material shows a propensity for forming bubbles. Nevertheless, leak-tight seals can be achieved with a minimal wall strength of solder as little as 100µm. This result boasts confidence in our bonding approach and suggests that with some process engineering it should be possible to implement this technology successfully on a larger scale.

Solder microstructure and stability

During our limited experience with activated tin solder materials we have observed aging of Al and Mg containing solder alloys. This aging must be investigated further, thus far the exact mechanism is still unknown. Our observations with activated solder alloys are the following:

- Embrittlement of solder alloys can occur with time and has been observed in a few cases. This is evidenced in a complete loss of ductility which tin normally possesses. Solder materials are prone to breaking and or disintegration.
- The porosity of the metallic phase increases visibly with embrittlement and loss of mechanical integrity.
- Along the fractured interface, the metal looks greyish (oxidized ?, α tin ?).
- The embrittlement effect appears more pronounced with alloys of higher Al, Mg content
- Coalloying with other structure-modifying metals (Ag, Cu) seems to yield improved properties or resistance against embrittlement.
- The cooling speed of the liquid solder melt seems to affect the embrittlement rate.
- In addition to embrittlement, we also observe the formation of bubbles inside the solder which are most likely due to outgassing of dissolved gases from the liquid metal in vacuum.

From these observations, we postulate that a microstructural change is prone to occur in Al and Mg activated solder materials over time. This change is probably initiated or catalyzed by the formation of new grain boundaries during solidification of the melt. Tin does not form any intermetallic compounds with Mg and Al in that composition range, and hence the activating metals will precipitate during solidification of the liquid alloy and form homogeneously distributed metal islands /particles along the receding grain boundaries. This can be validated by SEM/EDS analysis.

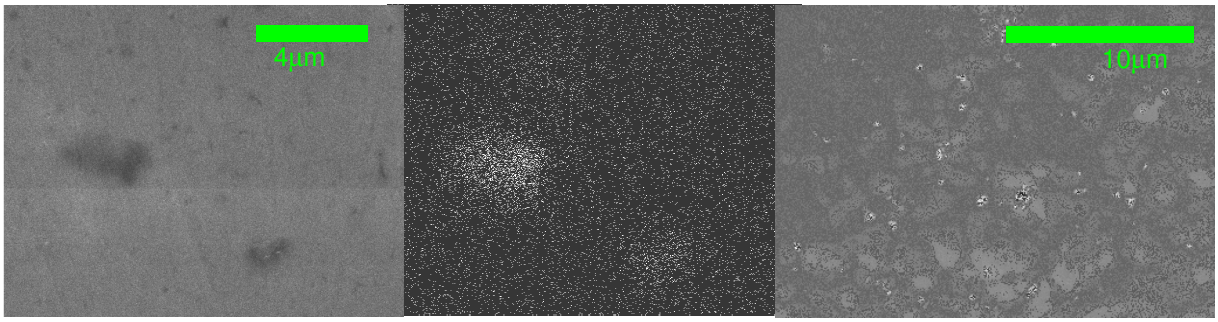

Fig. 28 SEM images (left and right) and Al EDS element distribution map of a SnAl0.5‰$_m$ polished alloy surface. Note that surface etching greatly enhances the image quality (SE image on the left)

The left and center image in Figure 28 show SEM image and the corresponding Al element EDS map of a cut and polished embedded solder sample. Two larger Al grains are clearly visible in both images. The right-hand image show much improved detail such as grain boundaries and Al precipitates after etching with an ion-milling device. One of the most plausible explanations for the observed changes and embrittlement is that these activating metal grains foster or initiate the phase change from white β tin to grey α tin. The tin-pest affinity could be reduced by addition of Sb, Bi, Ag or Pb. An in-depth study which is looking at the cooling rate dependent metal microstructure and related interfacial defects in grain boundaries detected by positron annihilation is currently on its way.

Additional optimizations such as a detailed study of the effect of activating components on the workability, bonding performance, strength and durability of the resulting alloy will be carried out in the future. Other possible alloying elements such as Li, Be, Ga, and In and combinations of these must be tested as well. Of equal importance is the effect of the type and amount of co-alloying elements used on the bonding performance and alloy durability and its mechanical properties.

Summary, outlook and additional investigations

We have demonstrated the ability to fabricate leaktight seals with anodically bonded specimens using thin Al-foils early on. Aluminum frames made from 250µm strong sheets i.e. of a thickness which corresponds to a typical vacuum glazing cavity gap width, cannot be bonded anodically without macroscopic channels or leaks. For this reason, an alternative sealing approach – anodic bonding of liquid solder alloys – was pursued. Common lead free solder alloys such as SnAg3.5%$_m$ and SnAg3.0Cu0.5%$_m$ show improved contact with and adaptation to the glass surfaces but a large amount of bubbles and mechanically weak, leaky seals. The addition of an activating metal to the solder alloy such as Al or Mg significantly increases the mechanical strength of the anodic bonding seal. Using a SnAl0.5%$_m$ soft solder alloy, we were able to produce a 5cm by 5cm anodically bonded specimen with a bonding time of only 90 seconds which was leaktight (leak rate below detection limit of the He leak testing device) and mechanically durable.

Generally, we observe that workpieces made from soft solder alloys will exhibit a partially oxidized area of contact and inferior bonding strength at the original workpiece/glass contact when bonded anodically. In addition, liquid solder can be squeezed out under mechanical loading which forms a new, native area of contact with the glass which bonds significantly more strongly, is mirror-like in appearance and virtually free of bubbles or other defects. The goal is now to produce fresh, squeezed out solder/glass anodic bonds and upscale this technology for vacuum glazing edge sealing.

Our current objectives of the liquid phase anodic bonding method development are oriented towards two main goals: First to find an improved alloy composition which does not age or degrade, remains soft and malleable over time and shows good performance for anodic bonding. The secondary focus is to determine ideal bonding conditions for various alloys. A set of additional experiments is planned to further investigate the exact bonding mechanism with the goal to clearly differentiate between electrochemistry and ion migration in an electric field leading to a uniform theory of anodic bonding with liquid (activated) solder alloys.

Numerical analysis of heat transfer over the entire glazing assembly

A significant reduction in the heating energy demand of buildings can be achieved by lowering the thermal transmittance of glazing systems. Our work in the domain of numerical analysis and assessment of the energy saving potential of evacuated glazings is briefly summarized here. For a more detailed description of our work in this field, the reader is referred to the publication by Manz[3]. This article reviews all the relevant heat transport processes which occur in gas-filled and evacuated insulating glazing cavities and systems.

In a gas-filled cavity heat is transferred by radiative exchange between the glass pane surfaces, convection and gaseous conduction. The use of two low-emissivity coatings ($\varepsilon = 0.04$) lowers the heat transport due to radiation between the glass pane surfaces to roughly 0.1 $W \cdot m^{-2} \cdot K^{-1}$. If fill gases such as krypton or xenon are used, thermal conductance due to convection and conduction can be reduced to a value slightly below 1 $W \cdot m^{-2} \cdot K^{-1}$. Heat transfer by convection and gaseous conduction are only negligible if the cavity is evacuated to a pressure of about 10^{-2} Pa. Heat transfer is then determined by radiation and, more importantly, conduction through support pillars which are required to bear the atmospheric load impinging on the external pane surfaces. Even though average centre-of-glazing heat transfer rates which are some two to five times lower than those of gas filled cavities are theoretically possible for evacuated glazings, the significance of heat transfer in the glazing edge regions cannot be neglected and depends strongly on the size of the glazing. The impact of the edge seal and different frame constructions on the glazings thermal transmittance was modeled numerically.

Our results agree with those of other previously published studies and suggest that the evacuated glazing concept offers significant advantages over current technology in terms of overall thermal transmittance.

Numerical analysis of the mechanical behaviour of the glazing assembly

Mechanical loading of vacuum glazing occurs mainly due to atmospheric pressure and temperature differences between inside and outside air resulting in a differential thermal expansion of the internal and external glass panes. A series of static nonlinear finite element analyses for vacuum glazing with surfaces up to 3 m × 3 m and glass pane thicknesses between 3 and 10 mm were conducted, using three different styles of finite element modeling of the glazing. Assuming uniformly distributed glass-pane temperatures, and unlimited glass strength the deflection values obtained by different modeling styles for identical glazing geometries were in good agreement. The study further revealed that for large glazing surfaces and glass-pane temperature differences the deformation behavior is strongly nonlinear as it is apparent in the plots in Figure 29. It was further suggested that contribution of the support pillars to the transverse shear stiffness of the glazing assembly has to be taken into account when trying to predict the over-all glazing deflection.

Consequently, for the design of large-area glazings, a scaling or extrapolation from smaller geometries is hardly possible but non-linear analysis methods are required. In the linear limit neither the glazing deflections nor the stress distribution in the edges can be predicted adequately. The paper entitled “Finite Element Analysis of Temperature-Induced Deflection of Vacuum Glazing”[20] describes our results in more detail.

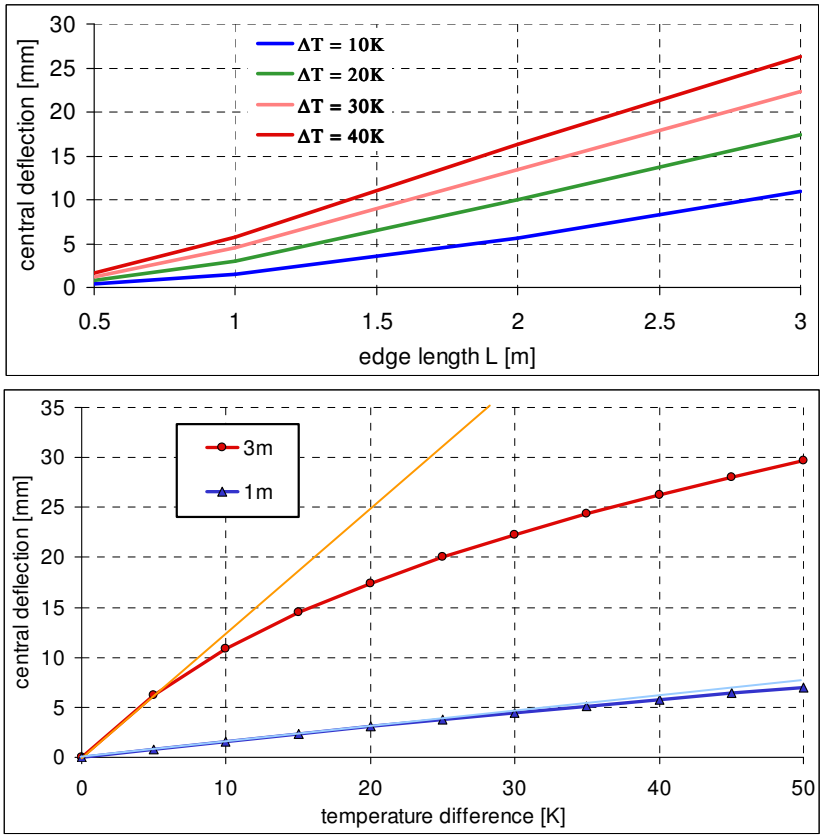

Fig. 29 Predicted central deflection as a function of edge length for four different temperature differences ΔT (top) and central deflection as a function of the ΔT value (bottom) indicating strongly nonlinear behaviour.

Service life analysis based on leakage measurements of prototype assemblies and simulations

One central question governing the practical applicability and eventually chance for success of any commercial products is that of the service life: If a pressure of 10^{-2} Pa is to be maintained over a typical lifetime of 30 years or more, no significant pressure increase should occur during that time if the thermal insulation performance is to be maintained. A number of publications on this topic exist in the literature; however the majority of them deal with the consequences of the non-ideal or inferior nature of the glass-solder sealing technology, which is by far the most commonly used technology, in combination with evacuation through a pumpout port. To the best knowledge of the authors, our work is the first to use a phenomenological approach to describe the service life in terms of different sources of pressure increase. We propose the following four sources as relevant contributions to transient pressure increase (aging):

- Permeation of small gaseous molecules (air constituent), particularly Helium
- Leakage through the edge seal
- Thermal and optical desorption of organic adsorbate species
- Photogfragmentation reactions of large adsorbate molecules

Eventually, the sum of all four contributions must not cause a pressure increase inside the cavity greater than 10^{-1}Pa after 30 years. Alternatively, the use of getter materials can reduce the pressure buildup, however the gettering efficiency strongly depends on the type of molecular species to be trapped. Helium for example cannot be gettered because of its inert character. In this work we present a set of parameters and define numerical constraints which must be satisfied in order for the cavity pressure to be maintained over a minimum period of 30 years. Figure 30 shows a schematic of an evacuated glazing and the different sources of pressure buildup 1) through 4) as well as the getter (or chemical trap) 5).

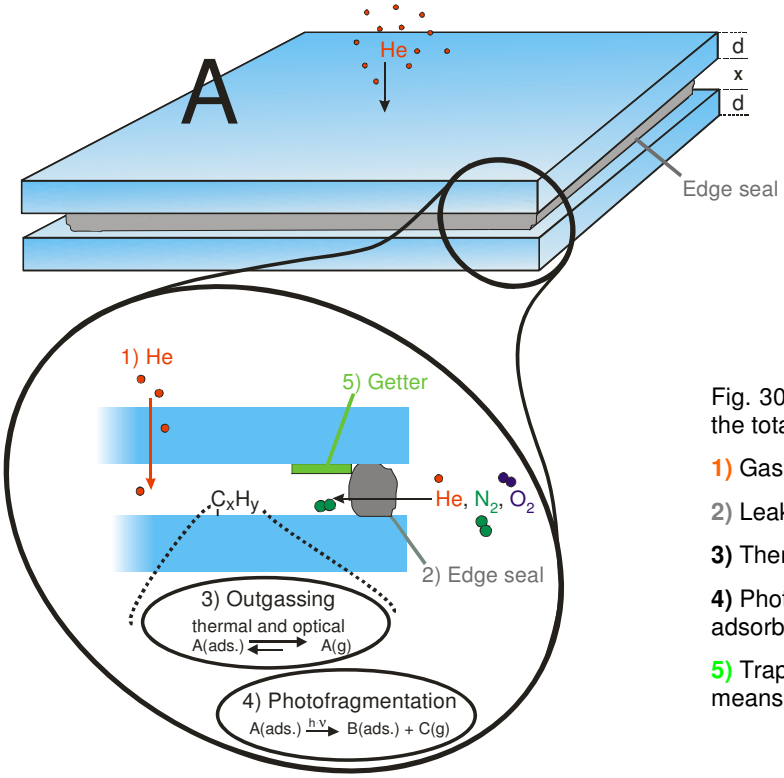

Fig. 30 Schematic illustrating contributions to the total pressure buildup

1) Gas (He) permeation)

2) Leakage though the edge seal

3) Thermal and optical desorption (outgassing)

4) Photofragmentation reactions of organic adsorbates and

5) Trapping of certain chemical species by means of a getter material

Before treating life-time related aspects in more detail, the reader must be reminded of the prodigious nature of and requirements on the evacuated cavity vacuum chamber. Typical high-vacuum chambers which are commonly used in research have a volume of a few tens of liters and an inner surface area below one square meter. Our calculations are based on a typical “large” evacuated glazing of 2m by 3m dimension consisting of two 6mm strong glass panes with an evacuated gap x of 0.2mmmade from various glasses. This vacuum glazing system exhibits a roughly 100 times larger surface-to-volume ratio than the typical HV chamber mentioned above. On the other hand, the reduced dimensionality (the glazing is a quasi two-dimensional system), the mean free path of the gaseous species is by far longer than the gap width, which increases the time an average molecule spends adsorbed on either side of the glazing surface when compared to the time in the evacuated volume. Still, it is an enormous achievement to keep an evacuated glazing system at a constant pressure of 10^{-2} Pa without additional pumping. It is because of the immense contribution of the surfaces that desorption and fragmentation of organic adsorbates play an important role and cannot be neglected in a pressure-lifetime balance.

Permeation of gas molecules through the window panes

Permeation of small molecules through various glasses was extensively studied in the 1950ies. Permeation rates for various glass types were taken from literature data[21,22] and corrected for any desired temperature by means of an Arrhenius correction term. Starting from the permeation rates, transient mole amounts of different gaseous species were calculated given the sample geometry of the model glazing. The resulting pressure increase was evaluated using the ideal gas law. In addition, a model by Todd[23] was used to estimate the transport of water vapour through the glass.

Due to its small size and weak chemical interaction with its surroundings, He diffuses by far the most rapidly through glasses when compared with other gaseous compounds. The permeation rate of He through various glasses is roughly 6 to 7 orders of magnitude larger than those of the main air constituents nitrogen and oxygen. This is how Helium, despite its minute concentration in ambient air of only 0.0005% by volume, becomes the major component in ambient air permeating through float glass to the extent of a full 92% followed by Neon with approximately 6%. Therefore, the phenomenon of ambient air permeating through glasses at low pressures is often referred to as helium permeation. Remarkably enough, at cavity pressures of 0.1 Pa or lower, the main constituents of ambient air, N_2 and O_2, make up for only 2% of the total as it can be seen in the chart shown below in Figure 31.

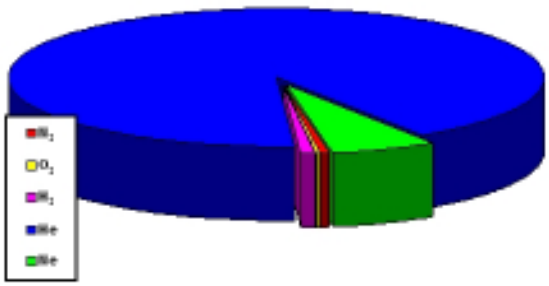

Fig. 31: Pie chart graphic representation of the relative contribution of the main contributing gas species to the total pressure increase due to gas permeation in vacuum glazing in its initial stage. Helium is clearly the most rapidly permeating species with a > 90% contribution followed by Neon.

Perhaps the central question is that of the transient He-permeation and the resulting pressure increase inside the cavity. From our model calculations we can conclude the following: First, there are very large differences in the permeation rates depending on the glass composition as seen in Figure 32. Surprisingly enough, float glass (or soda-lime glass) is the ideal material for the manufacture of evacuated glazings: it combines low cost, good workability and low gas (He) permeability. Phosphate glasses could be a reasonable alternative, however they may not be suited for anodic bonding edge sealing. Glasses with a low network modifier (Na, K, Ca, Mg) content such as pyrex or fused silica (red and orange lines), exhibit far higher gas permeabilities than float glass leading to very large transient Δp values. Note that the slope of the transient curve is changing above approximately 0.5Pa, a point which will be discussed further. Figure 32 shows the transient pressure increase calculated for a constant temperature of both panes of 20°C and 50°C using our model.

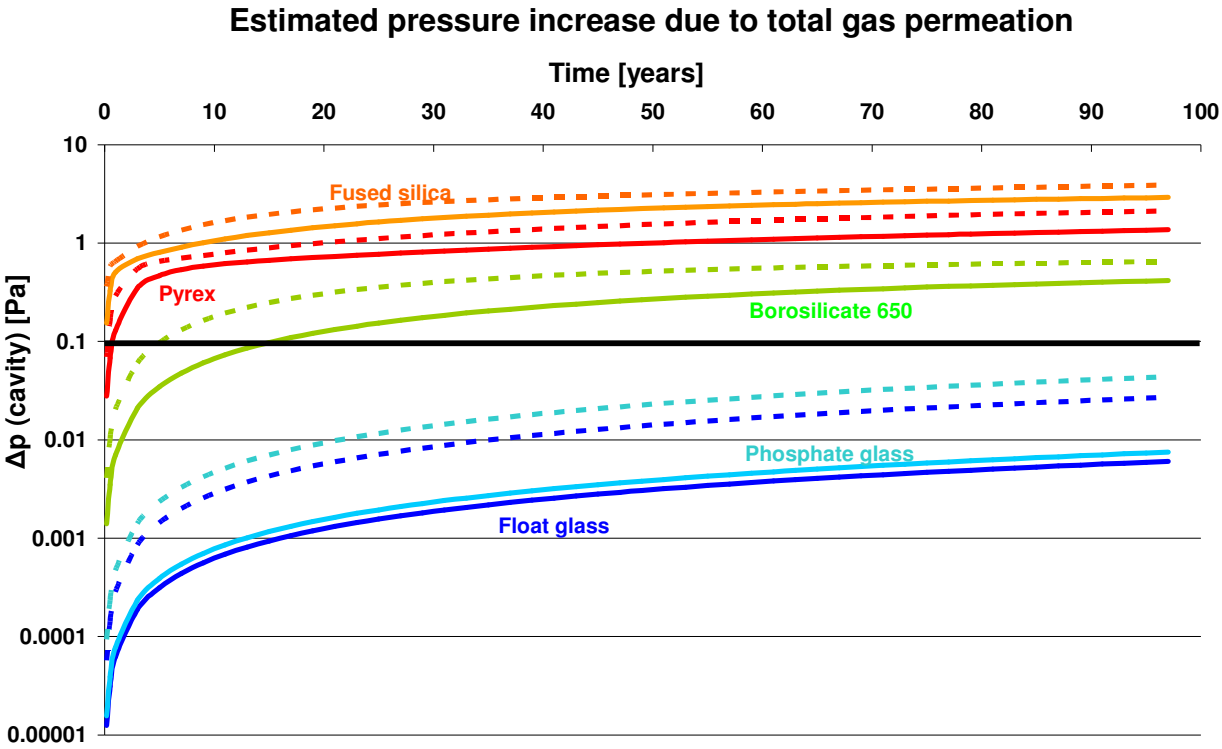

Fig. 32: Estimation of the gas-permeation induced pressure increase in a vacuum glazing with 6mm thick panes made from different glass materials. Transient results based constant panes temperatures of 25°C and 50°C.

The thick, black horizontal line marks the critical pressure of 0.1Pa which must not be breached for an unimpaired insulation performance. For float glass (Soda lime glass 0080, blue line) it is shown that the pressure increase at both 25°C and 50°C due to the combined permeation of the gases He, Ne, N_2, O_2 und H_2 does not reach the critical level even after a period of 100 years. A second scenario under worst-case conditions is significantly more rigorous: For one pane at a constant temperature of 20°C and the other at 80°C, a resulting pressure increase after 30 years of 0.087 Pa is predicted. In addition to gas permeation from air constituents, the permeation of water was also estimated using Todd's model. Compared to He, the permeation of water vapor is of small relevance; assuming a constant temperature of both panes of 60°C, a pressure increase due to the latter of only 0.003 Pa after 100 years would result. Even though in the case of float glass, permeation does not pose an immediate threat to the glazing performance, the integrity of a glazing assembly under such thermal loads is of great concern and must be studied separately.

The change in slope of the transient Δp curves was mentioned above. It is due to the fact that the effective pressure difference varies for each gas depending on its permeation rate and the relative abundance in ambient air. The ambient partial pressures of Ne, He and H_2 are 1.82, 0.51 and 0.05Pa respectively. If a glass material is permeable enough and the atmospheric partial pressure for a gaseous species is low enough, the effective pressure difference for either one of these three compounds between in- and outside of the cavity can approximate zero. In other words, at some time the system reaches an equilibrium situation with respect to permeation of a certain compound. From that time on, there will be no further net diffusion of this species into the glass and that gas will therefore seize to contribute to the total pressure increase. This is shown in the case of Pyrex glass at 25°C in Figure 33 below.

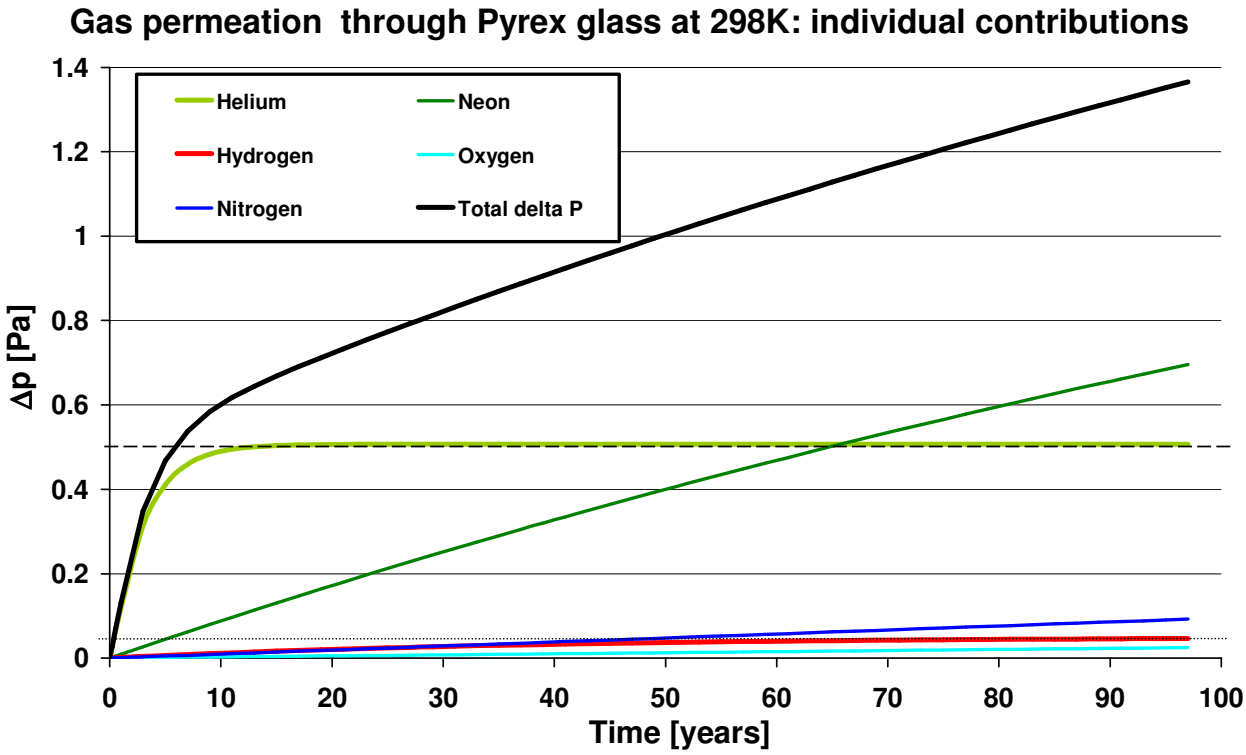

Fig. 33: Transient pressure increase function for Pyrex glass at 25°C showing the contributions of the different permeating gases He, Ne, H_2, N_2 and O_2.

During the first three years, the main pressure buildup is due to permeation of He. After that time, the Helium partial pressure inside the cavity is close to its atmospheric one which heralds the end of He role as the leading permeating species: From approximately 10 years on, Neon becomes the main source of pressure increase and it will continue to do so until it is as well in equilibrium with the ambient atmosphere (at around 1.82 Pa, not shown here). Note that hydrogen reaches its equilibrium cavity pressure of 0.05Pa after approximately 50 years. Once He and Ne reach their equilibrium pressure inside the cavity (at around 2.4Pa depending on temperature and the permeated oxygen and nitrogen amounts), the pressure increase is dominated by nitrogen and oxygen permeation only and from this point on the pressure gains are significantly slower. This is also seen in the transient curve for fused silica (orange line) in Figure 32.

The critical pressure which must not be breached during a typical service life of 0.1 Pa is in the regime which is dominated by He permeation. Hence, it is reasonable to assume that permeation of He gas into the glazing cavity is lifetime limiting. In the case of float glass, the permeation rates are low enough, that diffusion of gases (particularly He) are in no way life-time limiting, if a glass thickness of 6mm or larger is used.

Leakage through the edge seal

The leakage through the edge seal is the parameter of central importance to the glazing and is entirely sealing technology dependent. Losses due to a leaky edge seal are easily several orders of magnitude larger than ones from any other source. In other words, failure of the edge seal right after assembly or with time will be fatal to the glazing unit. For this reason, finding and choosing a sealing technology suitable for mass-production is of utmost significance and will decide over success or failure of the final product: To date, there is no technology available yet which is industrially used and satisfies all criteria of an ideal sealing technique as defined on page 8 (The ideal sealing approach).

A leak is the effluence or penetration of gas molecules through channels or cracks between two sides of an object where, in analogy to permeation, the driving force is an external pressure difference between the two sides. In vacuum technology, leaks are often classified based on their respective transport or flow mechanism: leaks with viscous gas flow (macroscopic leaks) exhibit leak rates > 10^{-4} mbar $\cdot$ l^{-1} $\cdot$ s^{-1}, ones with molecular gas flow (fine leaks) rates below 10^{-7} mbar $\cdot$ l^{-1} $\cdot$ s^{-1} and last but not least, leaks with gas permeation (typical examples are permeation through interatomic spaces in polymers or elastomers, sealing rings etc.) with leak rates[24] smaller than 10^{-7} mbar $\cdot$ l^{-1} $\cdot$ s^{-1}. The magnitude of a permeation leak is strongly dependent on the materials molecular structure and the geometry of the workpiece under investigation. If we consider leakage through a vacuum glazing edge seal, only the first two modes of leakage are relevant. In other words, if an edge seal is produced with no macroscopic or fine leaks present, the residual leak rate is due to permeation of gases through the metallic seal only. Permeation through metals is intrinsically small. In the case of our tin-based edge seal, the favorable geometry (thin gap width combined with centimeter width of the seal) further reduces the effective permeation rate. For this reason it is relatively safe to assume that a seal with a leaktightness or hermeticity better than the limit of detection < 10^{-10} mbar $\cdot$ l^{-1} $\cdot$ s^{-1} also has a leak rate which satisfies the commonly quoted leak rate requirement of < 10^{-12} mbar $\cdot$ l^{-1} $\cdot$ s^{-1}. For a 2m $\times$ 3m evacuated glazing with a 200µm gap width, such a leak would cause a pressure increase of less than 0.08 / 0.26 Pa after 30 / 100 years respectively. Testing of edge-sealed specimens was typically conducted on 5cm by 5cm samples, with a 3mm hole in one of the glass pieces. In the absence of macroscopic or fine leaks, leak rates < 10^{-10} mbar $\cdot$ l^{-1} $\cdot$ s^{-1} in He were measured which is also the detection limit of our leak testing device. In principle there exist more sensitive leak rate measurement devices with detection limits[25] downto $2 \cdot 10^{-13}$ mbar $\cdot$ l^{-1} $\cdot$ s^{-1}, however the use of such instruments is questionable for reasons of accessibility, cost and arguable benefit as stated above.

Additional complications could of course ensue over time due to aging of the edge seal. Cyclic mechanical and/or thermal loading can cause damage with time for example in the form of microcracks or delamination locally or over larger areas. For an improved risk assessment of this problem, cyclic mechanical loading tests should be performed on 0.5m $\times$ 0.5m glazing prototypes. Such experiments will show, if the edge-sealing approach developed in our laboratory can withstand real-life conditions without failure. Testing of larger prototypes is also a main field of interest of future activities.

Desorption of organic compounds through thermal and optical irradiation

Optically and thermally induced desorption (outgassing) of adsorbate molecules (water, CO, CO_2, small organic molecules) is based on the equilibrium between surface adsorbed and free gas phase molecular species A according to

$$A\ (ads.) \underset{}{\overset{K}{\rightleftharpoons}} A\ (g)$$

where K is the equilibrium constant in the traditional sense of chemical kinetics and describes the ratio of forward and backward reaction rates. This equilibrium is a function of temperature and pressure meaning that at high temperatures and low pressures, the left side or gaseous products are favored. Adsorption/desorption phenomena are key in the HV and UHV pressure regions giving rise to the large surface contributions to the total system pressure and have been extensively studied, also in their adapted form as it is relevant in vacuum glazing: Numerous scientific publications on this topic describe the outgasing process in evacuated glazing prototypes[26,27,28]. All those studies relate the thermal and/or optical irradiation with the pressure increase within the cavity measured by a spinning rotor gauge and the desorbing species which were identified by mass spectrometry. For surface analysis and mass spectrometry, a rather complicated experimental setup is necessary which requires in-situ breakage of sealed specimens in a high vacuum measurement chamber and consequent analysis of desorbed gases. All those studies have shown that specimens sealed with glass solder

- and baked at 150°C prior to and during evacuation through a pumpout tube outgas significant amounts of H_2O, CO und CO_2 when subjected to a heat treatment or UV exposure.
- and baked at temperatures between 320°C to 350°C prior to and during pumpout, little to no outgassing of said molecules was observed upon UV irradiation or heating.
- when in contact with ambient air showed immediate contamination by organic adsorbate molecules (XPS surface analysis)[29,30].

These results are generally known already from standard vacuum technology baking and outgassing procedures. Nevertheless, the demonstration of their validity for evacuated glazing systems is essential. One common factor which collates all those studies is the method of sample fabrication namely the glass soldering method with subsequent pumping through an evacuation port or pumpout tube. It is the use of this unfavorable technology that requires heating at temperatures above 300°C and long pumping times to guarantee complete outgassing of the inner glazing assembly walls. It is for this reason, that the desorption problem has received that much attention and that the topic of photofragmentation reactions has not been mentioned in the literature thus far. In contrast, the liquid solder based anodic bonding edge sealing method developed in our laboratory is a “seal and forget” technology and completely high-vacuum compatible. During the baking stage, prior to the bonding process, the two window panes are separated by a typical distance of 20cm and are only brought together at the last moment to the 0.2mm final separation defined by the support pillars. This means that during the outgassing process, the pumping speed inside the chamber is not artificially lowered due to the narrow glazing separation, especially at lower pressures. In other words, the final cavity pressure is the equilibrium pressure of the entire chamber at the specific baking temperature (typically 300°C or lower). Small molecules such as H_20, CO, CO_2, low-molecular aldehydes, carbonic acids, esters, amines etc. will be removed efficiently and rapidly prior the bringing together of the panes. This is because the respective equilibrium for small molecules lies strongly on the

side of the gas-phase under the conditions experienced prior to bonding (high temperature, low pressure and glass panes separated by ~20cm) and hence are efficiently removed from the system by vacuum pumps pumping action. No additional experimental studies on outgassing were performed in our laboratory.

Fragmentation of long-chain organic adsorbate molecules through optical irradiation

An altogether different topic is the possible fragmentation of long-chain aliphatic molecules such as tensides, silicones, and hydrocarbons on the glazing surface. Such compounds are omnipresent and adsorb more or less irreversibly on glass surfaces. It seems plausible that such molecules can decompose into smaller fragments through a variety of photofragmentation reactions. A single fragmentation step can be phenomenologically written as

$$\text{A (ads.)} \xrightleftharpoons{h \cdot \nu} \text{B (ads.)} + \text{C (g)}$$

with A being the original long-chain adsorbate molecule, $h \cdot \nu$ a UV photon, B the remaining adsorbate of reduced chain length and C a small molecule degradation product such as ethylene, acetaldehyde, acetic acid etc. Note that this reaction step can be repeated several times until the original adsorbate A is completely decomposed into small fragments. The degradation products C created in this way are volatile and spend significantly more time in the gas phase than adsorbed on the inner glass surfaces and therefore lead to a pressure increase inside the sealed cavity. From a practical point of view, a rough cleaning of the glass surfaces with an aqueous soap or detergent solution prior to assembly is quite indispensable to remove dust, impurities and contamination. Typical detergents contain long chain sulfonic acids or trialkylammonium compounds and perhaps nonionic tensides such as poly-(ethylene glycols). After a wet cleaning step with detergents, the presence of such substances on the surface cannot be avoided. UV irradiation of a polyethyleneglycol tenside as an example can produce acetaldehyde as a primary small molecule decomposition product in a completely inert vacuum atmosphere even under complete exclusion of additional reactants such as oxygen or hydrogen. If a surface were covered to only 5% of a monomolecular layer of such a polyethylene glycol tenside, the complete photofragmentation into acetaldehyde would bring about a pressure increase inside the cavity of more than 10 Pa! Even though the optical absorption cross section (the extinction coefficient) of UV light of hydrocarbons is extremely small, the incorporation of secondary atoms or functional groups such as amines[31] can yield a drastic increase in absorbance and hence in the probability of such degradation reactions taking place.

The complexity of both the variation of different adsorbates present on the surface (which is intrinsically linked to the glass pane history) and the possible photodegradation and recombination reactions is such that a detailed analysis is quite impossible. However, the use of model systems to investigate such processes could prove useful in estimating the overall relevance of photodegradation reactions. We strongly believe that the role of the photophysics and -chemistry of long-chain organic adsorbates is of central importance and imposes an artificial limitation on the service life of vacuum glazing units and therefore cannot be neglected. The obvious way to reduce the surface coverage of such adsorbates, and with it the potential for photofragmentation induced pressure increase, is the targeted removal by suitable surface cleaning methods. A potentially promising technique is UV/ozone surface cleaning which is known from the semiconductor industry[32]. A possible alternative which is used in the German Pro-VIG project is plasma sputter cleaning which is commonly

used for UHV cleaning of samples in surface science research[33]. The main drawback sputter cleaning is that precise control of the sputter rate is necessary in order to avoid "oversputtering" and damage to the low-ε multilayer system.

A series of experiments was conducted to assess the usefulness of the UV/ozone cleaning method: Low-ε coated glass (Silverstar NT, Glas Trösch) which had been equilibrated for several weeks in ambient laboratory air (Empa Dübendorf, Bauhalle) and precleaned using an aqueous detergent and isopropanol wash were analyzed by means of time of flight secondary ion mass spectrometry (TOF-SIMS). On all sample surfaces in contact with ambient air, some amount of organic adsorbate molecules were found. For the UV/ozone cleaning experiments, the previously measured "ambient contaminated" sample was placed inside a benchtop ozone generator (Novascan PSD-UV, unit operating with ambient air at atmospheric pressure) and exposed to UV/ozone for 10 minutes. Following the treatment, the sample was rapidly transferred in a glass container under inert atmosphere to the vacuum load lock system of the TOF-SIMS instrument, the system initialized and a complete secondary ion mass spectra sequence recorded for the second time.

For the model study experiment, a low-ε coated float glass specimen was decorated with a model compound sodium dodecylsulfate (SDS). To this purpose, the sample was rinsed with an aqueous/isopropanol solution containing 5mg/ml of SDS and the residual liquid blown off with dry nitrogen. Following this pretreatment, the glass was analyzed by means of TOF-SIMS and the presence of the SDS cation and characteristic fragments confirmed. In analogy to the ambient contaminated sample, a 10min UV/ozone cleaning was performed and the sample transferred and measured again. Figure 34 gives an overview of the results from the negative secondary ions datasets:

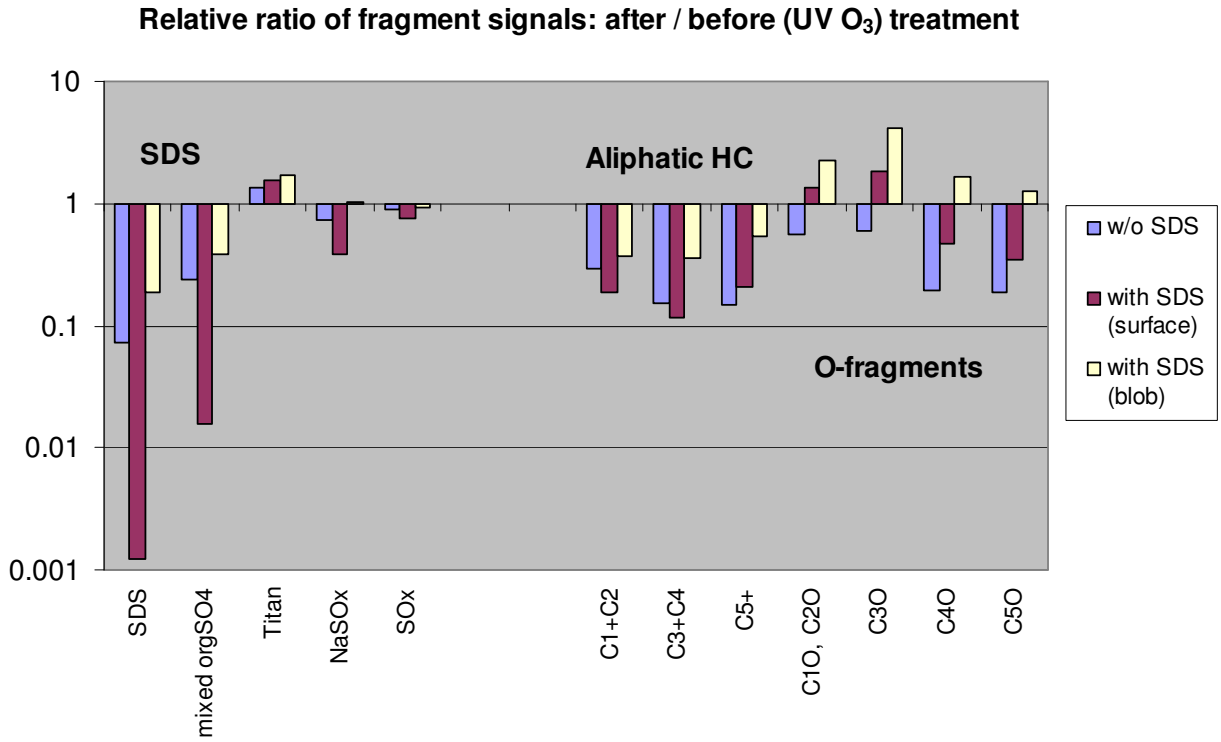

Fig. 34 TOF-SIMS analysis results of ambient contaminated (no SDS) and SDS decorated glass surfaces: relative negative ion fragment signal count after / before UV/ozone treatment

For all samples, more than 15 randomly chosen points were measured and the data shown here is a spatial average over all the measured locations. The ambient contaminated sample is represented by the blue bar (w/o SDS). For the SDS decorated sample, we differentiate between normal surface (wine red, “surface”) and spots or islands of dried SDS material (light yellow, “blob”). The distribution of SDS on the surface was quite homogeneous with exception of the spots or blobs, where the receding liquid front dried out and left behind copious amounts of material.

For the ambient contaminated sample we also see a signature of SDS, however the absolute intensity is very small (100 times less than for the SDS decorated sample) and only slightly above the background noise level of the signal before the ozone cleaning. After the treatment, the SDS fragment intensity is on the order of the background noise and can no longer be detected, hence the signal drop by about a factor of 10. More importantly, we find a variety of aliphatic and partially oxidized organic adsorbates (alcohols, ketones, carbonic acids) already present on the surface which are clearly due to ambient contamination. The hydrocarbon surface coverage is decreases by less than one order of magnitude after the ozone treatment, however also in this case, the absolute amounts of contaminants present on the surface before the ozone cleaning are comparably small. This indicates that surface contaminants are being removed by the surface cleaning process. The same trend can be observed for the partially oxidized species. In addition there is a clear trend in chain-length selectivity which means that longer chain molecules (C5+, C5O) are more efficiently degraded than shorter analogues.

So far we have established the fact that there are small amounts of hydrocarbons present on the surface and that they are being oxidatively removed in part by the ozone cleaning. A closer look at the more representative SDS (surface, wine red bars) signal in particular demonstrates nicely, that the model compound is being efficiently cleaned from the surface. This is reflected in a roughly three order of magnitude decrease of the SDS main fragment signal. In addition, mixed organic sulfates (possible oxidation products and fragments created during the TOF-SIMS analysis process) are reduced by two orders of magnitude. At the same time, the hydrocarbon fragments behave virtually identical as in the ambient contaminated case. They can be considered as a spectator background originating from an ambient contamination superimposed onto the SDS signals. The amount of partially oxidized fragments C4O and C5O still decreases but then increases slightly for the shorter chain ones (C3O, and C1O, C2O) indicating that larger byproducts of the long chain oxidiation process are not stable but are degraded to very small fragments. This observation is direct evidence of a complete oxidative removal of our model substance SDS. In the SDS spot areas (light yellow bars, “blob”), the thickness of the film of the spot itself is too large to be completely degraded during the given exposure time of 10 minutes. In this case, the amount of partially oxidized intermediates increases as expected.

The study presented here gives direct evidence of the complete degradation of a long-chain tenside model compound (SDS) decorated low-ε glass surface upon UV/ozone treatment: The main molecule fragment is reduced by three orders of magnitude and at the same time, no intermediate or long-chain products are accumulating on the surface. This suggests, that a rapid surface cleaning treatment can be devised based on this approach which eliminates the potential of pressure buildup by long chain adsorbate photofragmentation by roughly three orders of magnitude.

Use of getter materials

The need for a getter material arises, if the total pressure buildup, consisting of the sum of the four sources discussed above, within a 30 year service life period substantially exceeds a value of 0.1 Pa. Getters trap certain volatile chemical species in an irreversible manner and thus can lower the pressure in the evacuated space. In other words, a getter is a material with a large affinity for one or several types of (small molecule) adsorbate species. This irreversible adsorption finds practical applications also in the form of getter pumps in ultra high vacuum systems; one of the most prominent examples is the Ti-sublimation pump. Generally one differentiates between evaporable and non evaporable getter (NEG) materials. The latter has been reported as a getter material suitable for evacuated glazing applications[34]. For solder glass fabricated glazing units evacuated through a pumpout tube, the use of getters can probably not be avoided[35] and may not even halt the evolution of gases (mostly desorption and photofragmentation) or large amounts of getter materials may be necessary to do so. In our case, the central question is whether the use of getters is necessary at all. If the answer is yes, one needs to know what type of chemical species is the primary source of pressure increase and the type of getter and its capacity can be chosen accordingly. For example if leakage of the edge seal is the primary concern, a getter with high nitrogen, oxygen and perhaps water sorption capacity is ideal. If photofragmentation products need to be trapped, a different material with a high affinity for small organic molecules (CO, CO_2, ethylene, ethanol, acetaldehyde, acetic acid etc.) should be chosen. Note also, that He-permeation cannot be antagonized by the use of getter materials at all because its inert nature does not allow Helium to form an irreversible sorption bond with NEG or any other compound. Hence the getter system and amounts must be tailored to each individual vacuum glazing system and perhaps can be omitted altogether.

Summary

Based on our model calculations, the permeation of He is below the critical limit for evacuated glazing units made from standard float glass used under standard and elevated temperature conditions. Edge seal bonding specimens which were fabricated using the liquid-phase anodic bonding method exhibited leak rates below the limit of detection of the instrument i.e. $< 10^{-10}$ mbar $\cdot$ l^{-1} $\cdot$ s^{-1}. Thermal and optical outgassing is strongly design and sealing method dependent and should not be a key player if bonding is carried out in a high vacuum environment. The potential for photofragmentation induced transient pressure increase can be significantly reduced if long-chain organic molecules such as detergents or oils etc. are removed by means of suitable cleaning methods such as UV/ozone cleaning which is the one studied here. TOF-SIMS analysis showed a drastic reduction of the model primary mass peak signature of the model substance SDS upon a 10min ozone treatment. Further, a significant decrease in other long-chain hydrocarbons was observed, indicating that a the oxidative degradation goes more or less completely to small molecules which in turn are pumped off easily and hence will be removed from the system during baking in high vacuum.

To conclude, under consideration of ideal process conditions, it should be possible that all sources of pressure increase are kept within a limit such that the total pressure buildup after 30 years is below 0.1Pa. In this case, the use of getter materials becomes expendable. Again, this is only realizable if an *in vacuo* sealing method is chosen.

Fabrication of a roughly 0.5m x 0.5m prototype glazing assembly including support pillars and getter

The planning of a High Vacuum prototyping chamber began in 2007. The idea was to design and construct a system which was able to produce a single evacuated glazing in one step of 0.5m by 0.5m dimension. For this purpose, a 25" cubic vacuum chamber with turbomolecular pump was custom ordered and built by ABBESS instruments, Holliston, MA, USA. The chamber itself has a cooling loop to prevent raising of the wall temperature which can be deteriorate or damage the rubber seal of the chamber door. There are two Al electrode plates which are heated by means of four resistive heaters of 400W peak power per plate. In addition there is a type K thermocouple on each heater to verify the temperature distribution of the electrodes. The upper electrode is hanging from the top and can be raised and lowered by a linear HV-feedthrough (Figure 35). Control and monitoring of the electrode heating and temperature as well as the high-voltage power supply voltage and current is done through a computer interface and a desktop workstation.

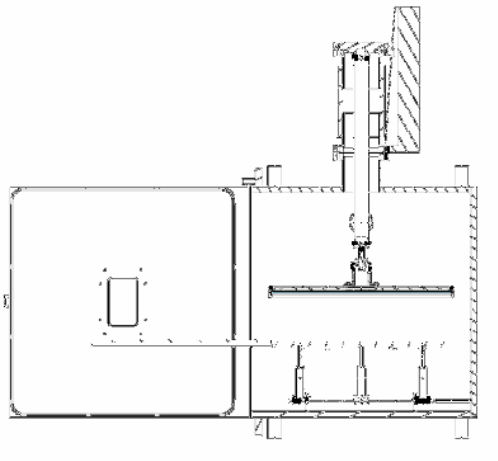

Fig. 35 2D layout of the prototype chamber

This chamber was constructed and tested for its functions in the spring of 2008. Three photographs of the chamber and its interior are shown below in Figure 36.

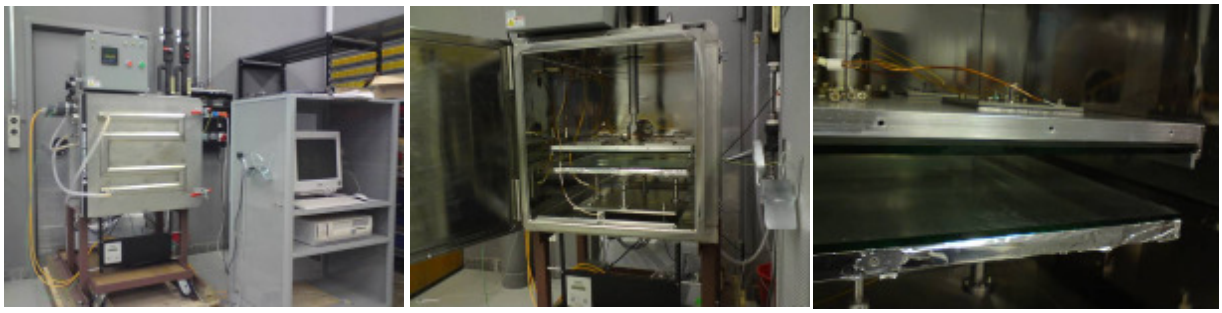

Fig. 36 Images showing the entire prototyping system including controls (left), the interior of the HV chamber (center) and the heated Al electrodes with mounted glass panes (right).

Following a series of chamber characterization tests (lowest pressure achieved, ideal heating rate etc.), the fabrication of prototype specimens was envisaged. Our first and only experiment so far was conducted in the following way: Two glass panes were cleaned and positioned with an array of 250mm high spacer pillars and a circumferential solder wire frame placed on the bottom pane and contacted. This frame had been extruded from an ingot of custom fabricated SnAl0.6%$_m$ alloy by means of the solder dispenser shown in Figure 37 prior to the beginning of the experiment and soldered together from multiple pieces with a standard solder iron without flux. The initial separation between the two plates was chosen to be 15 cm.

The chamber was then sealed and pumped to a base pressure of $< 2 \cdot 10^{-4}$ mbar. At this point, the chamber cooling loop was turned on and both electrodes were heated at a constant rate of ~ 1.5℃ · min^{-1} to the desired final sealing temperature, which in this case was only 240℃. Next, the upper plate was lowered onto the lower one by means of the linear stage and the anodic bonding process initiated by applying a voltage of 1000V between the Al electrodes and the liquid solder seal. After 6 minutes, the bonding voltage was turned off and with it the heating of the electrode plates. The sample was then allowed to cool to room temperature (>12hours) with the vacuum pumps still on, the chamber vented and the prototype sample removed from the system.

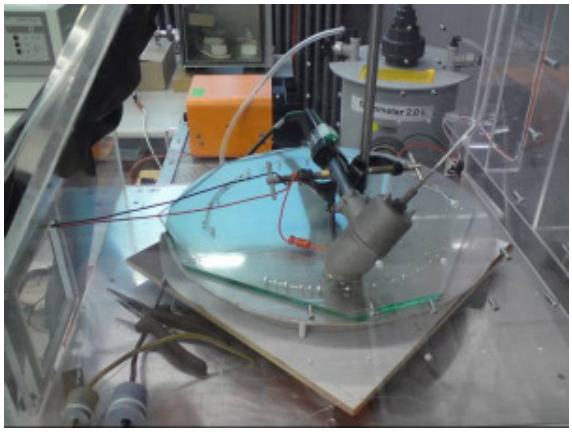

Fig. 37 Manufacture of solder wire used for prototype edge sealing from activated solder ingots by means of extrusion of liquid metal in an inert gas atmosphere

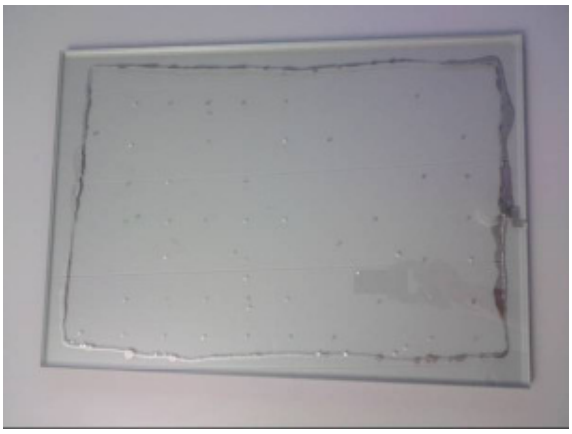

Fig. 38 First 50 cm by 30 cm sealing prototype manufactured in the large high vacuum chamber.

Figure 38 shows our first VG sealing prototype fabricated using the liquid solder anodic bonding technology. The seal is coherent along the entire perimeter but shows several large defects and is certainly not leak tight. However the specimen holds together and the seal appears mechanically robust. Due to the lack of sufficient amounts of long pieces of solder wire, we were unable to produce additional samples. This prompted us to shift our main research focus on optimizing the solder dispensing technology with a preferred method of realization being direct injection of liquid solder. On the plus side, we were able to demonstrate the ability to upscale the process from small to medium scale, however conditional on improvements of solder dispensing technology. Improvements in this field have a great potential to reduce the formation of defects, bubbles and oxidized, weakly bonded areas and will allow us to produce and test completely evacuated prototype specimens in this way. Prototype manufacture is an essential component of the follow-up project.

Summary, future activities and outlook

The vacuum glazing project has come to an overall successful completion and within the originally proposed timeline. All of the project tasks were completed with exception of the last one which was only partially completed due to difficulties with solder processing. A short summary with highlights of the individual milestones is listed below:

- We have developed the liquid solder anodic bonding technique with activated tin-solder materials for fabricating an edge seal with sufficient hermeticity good mechanical strength. The technology was filed for patenting in 2008. The integrity of larger seals remains to be tested and the solder bonding system optimized for large scale manufacture and maximum durability and strength.
- A numerical analysis of heat transfer over the entire glazing assembly was performed and the results published. Our findings agree with ones published in the literature and expands on aspects of pillar distribution as well as geometry and edge effects.
- The mechanical behaviour of the glazing assembly was studied using finite element analysis and, within the rigid edge seal assumption, showed a strongly nonlinear behaviour of stresses and deflection amplitudes with increasing glazing dimension and temperature.
- A systematic and complete service life analysis description of vacuum glazing was postulated for the first time. Our model takes into account four sources to the total pressure increase and one possible sink, the getter. A qualitative analysis of the individual sources reveals a set of parameters which will ascertain a 30 year service life of the glazing without performance loss.
- For the fabrication of up to 0.5m by 0.5m prototype glazing assemblies, a vacuum sealing chamber was designed, built and tested. A 0.5m by 0.3m prototype was fabricated using the liquid solder anodic bonding method. The assembly of additional prototypes was impossible because of difficulties with solder processing.

Challenged by the problematic of solder processing and dispensing, the idea of a follow-up project was created. A proposal was put together and submitted to EKZ (Elektrizitätswerke des Kantons Zürich). We were fortunate enough to be granted the support and are now in the process of setting up additional infrastructure for systematic solder dispensing investigations. This follow-up project is scheduled to run until the fall of 2010 at which point we hope to have optimized solder related aspects and established mechanical stability of 0.5m by 0.5m prototypes during standard glass testing procedures (with Glass Trösch AG) so that a CTI project for further upscaling to the industrial pilot scale can be envisioned.

Acknowledegements

The authors would like to thank the Swiss Federal Office of Energy (BFE) for funding and Dr. Nick Bosco, Prof. Dr. Jolanta Janczak-Rusch, Prof. Dr. Hans-Josef Hug, Dr. Hans Rudolf Elsener, Dr. Venkatesh Sivasubramaniam, Dr. Samuel Brunner, Dr. Beat Keller, Dr. Karl Emanuel Mayerhofer, Vinzenz Bissig, Stephan Carl, Roger Vonbank, Beat Margelisch and Rudi Blessing for various stimulating discussions and support with instrumentation and materials.

References

[1] http://www.energiestiftung.ch/energiethemen/energieeffizienz/gebaeude/

[2] If we assume a typical U-value of a double glazing of 1 $W \cdot m^{-2} \cdot K^{-1}$, roughly 5 times more heat is transmitted per unit area of glazed surface than through a newly constructed wall element with a typical U-value of 0.2 $W \cdot m^{-2} \cdot K^{-1}$ (corresponding to roughly 15cm mineral wool or styrofoam insulation)

[3] Manz, H.; *Renewable energy*, **2008**, 33 (1), 119-128

[4] Turner GM, Collins RE., *Int. J. Heat Mass Transfer*, **1997**, 40, 1437-1446

[5] Zoller, F; *German Patent #387655*, **1924**

[6] Gerspacher, *T.S.; US Pat. # 2398371*, **1944**

[7] Engel, D.; *US Pat. # 2658570*, **1957**

[8] Dunn, K. R.; *Int. Pat. # 1181656*, **1970**

[9] Manz, H.; Brunner, S.; Wullschleger L.; *Solar Energy*, **2006**, 80, 1632–1642

[10] Eames, P. C.; *Vacuum*, **2008**, 82, 717-722

[11] German ProVIG project: http://www.vig-info.de/

[12] Garrison, J.; Collins, R.E.; *Solar Energy*, **1995**, 55 (3), 151-161

[13] Griffiths P.W. et al., *Solar Energy*, **1998**, 63(4), 243

[14] G. Wallis, D.I. Pomerantz, J. Appl. Phys., 1969, 40, 3946

[15] Schjølberg-Henriksen, K.; Poppe, E.; Moe, S.; Storas, P.; Taklo, M. M. V.; Wang, D. T.; Jakobsen, H.; *Microsyst. Technol.*, **2006**, 12(5), 441-449

[16] Cheng, Y.-T.; Hsu, W.-T.; Najafi, K.; Nguyen, C.T.-C.; Lin, L.; *J. Microelectromech. Sys.*, **2002**, 11(5), 556-565

[17] Jousten K. (editor) ; *„Handbook of Vacuum Technology"*, ISBN 978-527-40723-1, **2008**, Viley VCH, Weinheim, Germany, pp 877-914

[18] Szabo, T. L. ; *"Diagnostic ultrasound imaging: inside out"*, **2004**, Elsevier Academic Press, Burlington MA, USA

[19] Sakaguchi, K.;Domi, S.; Nakagaki, S.; Suganuma, K.; *EU Pat. # EP1199289B1*, **2000**

[20] Wullschleger, L.; Manz, H.; Ghazi Wakili, K.; *Constr. Buildg. Mater.*; **2009**, 23, 1378

[21] Norton, F. J., *J. Am. Chem. Soc.*, **1953**, 36(3), 90-96

[22] Altemose, V. O., *J. Appl. Phys.*, **1961**, 32(7), 1309-1316

[23] Todd, J., *J. Appl. Phys.*, **1955**, 26(10), 1238-1243

[24] Nerken, A.; *Vak. Techn.*, **1958**, 7, 111

[25] Chen, X.; Huang, T.; Wang, L.; Jin, Q.; Cha, L., *J. Vac. Sci. Technol. A*, **2006**, 24(1), 91-94

[26] Ng, N.; Collins, R.; So, L., *J. Vac. Sci. Techn. A*, **2003**, 21(5), 1776-1783

[27] Lenzen, M. et al., *J. Vac. Sci. Techn. A*, **1999**, 17(3), 1002-1016

[28] N. Ng, R.E. Collins, *J. Vac. Sci. Technol. A*, **2000**, 18, 2549

[29] So, L.; Ng, N.; Bilek, M.; Pigram, P. J.; Brack, N.; *Surf. Interface Anal.*, **2006**, 38, 648

[30] So, L.; Ng, N.; Bilek, M., *Mater. Sci. Engin. B*, **2007**, 138(2), 135

[31] Machara, N. P.; Ault, B. S., *J. Phys. Chem.*, **1988**, 92, 6241-6245

[32] Seah, M. P.; Spencer, S. J., *J. Vac. Sci. Technol. A*, **2003**, 21(2), 345-351

[33] Taglauer, E.; *Appl. Phys. A*, **1990**, 51, 238

[34] Griffiths, P.W. et al., *Sol. Ener.*, **1998**, 63(4), 243-249

[35] Collins, R. E.; Simko, T. M., *Sol. Ener.*, **1998**, 62(3), 189-213